

1                   **Regulated release of cryptococcal polysaccharide drives virulence and**  
2                   **suppresses immune cell infiltration into the central nervous system**

3  
4  
5  
6                   Steven T. Denham<sup>1</sup>, Surbhi Verma<sup>1,2</sup>, Raymond C. Reynolds<sup>1</sup>, Colleen L. Worne<sup>1</sup>,  
7                   Joshua M. Daugherty<sup>1</sup>, Thomas E. Lane<sup>1</sup>, Jessica C.S. Brown<sup>1,3</sup>

8  
9                   <sup>1</sup>Division of Microbiology and Immunology, Pathology Department, University of Utah  
10                   School of Medicine, Salt Lake City, UT, USA

11  
12                   <sup>2</sup>Present address: Biochemistry Department, University of Utah School of Medicine, Salt  
13                   Lake City, UT, USA

14  
15                   <sup>3</sup>Correspondence: jessica.brown@path.utah.edu

16  
17  
18  
19  
20  
21  
22  
23  
24  
25  
26  
27  
28  
29  
30  
31  
32  
33  
34  
35  
36  
37  
38  
39  
40  
41  
42  
43  
44  
45  
46

47 **Abstract:**

48 *Cryptococcus neoformans* is a common environmental yeast and opportunistic  
49 pathogen responsible for 15% of AIDS-related deaths worldwide. Mortality primarily  
50 results from meningoencephalitis, which occurs when fungal cells disseminate from the  
51 initial pulmonary infection site and spread to the brain. A key *C. neoformans* virulence  
52 trait is the polysaccharide capsule. Capsule shields *C. neoformans* from immune-  
53 mediated recognition and destruction. The main capsule component,  
54 glucuronoxylosemannan (GXM), is found both attached to the cell surface and free in the  
55 extracellular space (as exo-GXM). Exo-GXM accumulates in patient serum and  
56 cerebrospinal fluid at  $\mu\text{g/mL}$  concentrations, has well-documented immunosuppressive  
57 properties, and correlates with poor patient outcomes. However, it is poorly understood  
58 whether exo-GXM release is regulated or the result of shedding during normal capsule  
59 turnover. We demonstrate that exo-GXM release is regulated by environmental cues  
60 and inversely correlates with surface capsule levels. We identified genes specifically  
61 involved in exo-GXM release that do not alter surface capsule thickness. The first  
62 mutant, *l/v7* $\Delta$ , released less GXM than wild-type cells when capsule is not induced. The  
63 second mutant, *cnag\_00658* $\Delta$ , released more exo-GXM under capsule-inducing  
64 conditions. Exo-GXM release observed *in vitro* correlated with polystyrene adherence,  
65 virulence, and fungal burden during murine infection. Additionally, we find that exo-GXM  
66 reduces cell size and capsule thickness in capsule-inducing conditions, potentially  
67 influencing dissemination. Finally, we demonstrated that exo-GXM prevents immune  
68 cell infiltration into the brain during disseminated infection and highly inflammatory

69 intracranial infection. Our data suggest that exo-GXM performs a different role from  
70 capsule GXM during infection, altering cell size and suppressing inflammation.

71

72 **Importance:**

73 *Cryptococcus neoformans* is a leading cause of life-threatening  
74 meningoencephalitis in humans. *C. neoformans* cells produce an immunosuppressive  
75 polysaccharide, glucuronoxylomannan (GXM), that is the main component of a  
76 protective surface capsule. GXM is also released free into extracellular space as exo-  
77 GXM, although the distinction between cell-attached GXM and exo-GXM has been  
78 unclear. Exo-GXM influences the outcome of infection, is the basis for current  
79 diagnostic tools, and has potential therapeutic applications. This study increases our  
80 basic understanding of the fungal biology that regulates polysaccharide release,  
81 suggesting that the release of cell-attached GXM and exo-GXM are distinctly regulated.  
82 We also introduce a new concept that exo-GXM may alter cell body and capsule size,  
83 thereby influencing dissemination in the host. Finally, we provide experimental evidence  
84 to confirm clinical observations that exo-GXM influences inflammation during brain  
85 infection.

86

87 **Introduction:**

88 *Cryptococcus neoformans* is a globally distributed saprophytic fungus found  
89 associated with certain species of trees and bird droppings (1). However, in  
90 immunocompromised humans *C. neoformans* acts as an opportunistic pathogen.  
91 Cryptococcal infections are responsible for 15% of acquired immune deficiency

92 syndrome (AIDS) related deaths worldwide, with most cases occurring in sub-Saharan  
93 Africa and Asia (2). Due to its global environmental distribution, human exposure to *C.*  
94 *neoformans* is almost universal (1, 3). Infections begin when inhaled fungal spores or  
95 desiccated yeast cells enter the lungs, where they are either cleared by the immune  
96 system, or contained and persist for a decade or more (4). Upon patient  
97 immunosuppression, *C. neoformans* cells can disseminate from the lungs to basically  
98 any organ in the body (5). *C. neoformans* proliferates particularly well in the brain,  
99 resulting in life-threatening meningoencephalitis (6). In fact, cryptococcal  
100 meningoencephalitis is a primary cause of death among HIV-AIDS patients, with  
101 mortality rates exceeding 50% in resource poor areas (2).

102 In contrast to many forms of bacterial and viral meningitis, cryptococcal  
103 meningoencephalitis is associated with strikingly low levels of inflammation and  
104 infiltrating immune cells into the central nervous system (CNS) of both human patients  
105 and mouse models (7-11). This paucity of inflammation is linked to poorer clinical  
106 outcomes, and subdued clinical signs that can delay treatment (9, 12, 13).

107 An essential factor for *C. neoformans* virulence is the conditional production of a  
108 thick polysaccharide surface capsule, which can more than double the diameter of a *C.*  
109 *neoformans* cell (14). The primary capsule constituent is glucuronoxylomannan (GXM),  
110 which comprises approximately 90% of the capsule mass (15, 16). Surface capsule  
111 plays a number of different roles during pathogenesis, protecting *C. neoformans* cells  
112 from phagocytosis, complement, and oxidative stress (15, 17, 18). GXM also has  
113 numerous immunomodulatory properties that facilitate fungal survival in the host (19).  
114 Notably, GXM increases anti-inflammatory cytokine (IL-10) release while dampening

115 proinflammatory cytokine release (IL-12, IFN- $\gamma$  TNF- $\alpha$ , IL-1B and IL-6) (20-23). GXM  
116 disrupts antigen presentation by macrophages and dendritic cells, and can even induce  
117 macrophage apoptosis, thereby diminishing T cell proliferation (21, 24-26). GXM can  
118 also suppress leukocyte infiltration into sites of inflammation (27-29).

119 GXM is non-covalently attached to the cell surface during cell surface capsule  
120 formation and maintenance (16). It is also found free within the extracellular milieu. This  
121 exo-cellular GXM (exo-GXM) reaches mg/mL concentrations in laboratory growth  
122 medium (30), and can be observed in the high  $\mu$ g/mL range in patient serum and  
123 cerebrospinal fluid (10, 31). GXM serum titers in HIV-associated cryptococcosis patients  
124 positively correlate with non-protective immune signatures and increased mortality (32).

125 Despite longstanding knowledge of the existence of exo-GXM, its connection to  
126 cell-associated GXM and the mechanisms behind its release remain largely unclear.  
127 One hypothesis has been that exo-GXM is shed mechanically from the cell surface  
128 capsule (16, 33). Alternatively, it has been speculated that distinct mechanisms might  
129 regulate the production of cell-associated and exo-GXM in response to environmental  
130 cues (15, 16, 34). This latter hypothesis is supported by observations that cell-  
131 associated and exo-GXM display different biophysical properties (34). Decreased  
132 electromobility of exo-GXM under capsule inducing conditions indicates that these  
133 differences could occur at the level of polymer length or branching (35-37).

134 Here we test the hypothesis that exo-GXM production is regulated by  
135 environmental conditions. We find that exo-GXM production is inversely related to the  
136 thickness of the cell surface-retained capsule and identify genes involved in these  
137 processes. Exo-GXM production also correlates with virulence and reduces infiltration of

138 immune cells into the CNS during infection. Together, these data support the idea that  
139 exo-GXM plays a critical but distinct role from cell surface GXM during infection.

140

141 **Results:**

142 Environmental signals alter exo-GXM levels

143 To investigate whether exo-GXM release is passive shedding of surface capsule  
144 or regulated at some level, we cultured wild-type *C. neoformans* cells for 24 hours under  
145 a variety of media conditions. We then measured capsule size and exo-GXM released  
146 into the medium. We chose both non-capsule inducing media and a series of capsule  
147 inducing media intended to produce a range of capsule induction. We harvested cells,  
148 then stained with india ink to measure capsule thickness as the distance from the cell  
149 wall to the outer capsule edge (**Fig. 1A**). We filtered supernatant through a through a  
150 0.22  $\mu$ m filter to remove cells, then visualized with immunoblotting with the monoclonal  
151 antibody (mAb) F12D2 to quantify exo-GXM release as relative staining intensity (**Fig.**  
152 **1B**). Exo-GXM band intensities were normalized to yeast nitrogen base (YNB) + 2%  
153 glucose levels, which was the condition with the greatest observed levels of exo-GXM.

154 We found an inverse relationship between capsule thickness and exo-GXM, such  
155 that cells growing in the strongest capsule inducing conditions, like 10% Sabouraud's  
156 buffered to alkaline pH, produced the least amount of exo-GXM (**Fig. 1A,C**). This  
157 relationship held across other capsule inducing conditions, such as nitrogen and iron  
158 limitation, that produce intermediate levels of both cell surface and exo-GXM.

159 GXM is an  $\alpha$ -1,3-mannan backbone with branching glucuronic acid and xylose  
160 residues and variable 6-O-acetylation on the backbone (38). O-acetylation varies across

161 strains, is not required for capsule formation, but significantly affects GXM's  
162 immunoreactive properties (38-40). Deletion of *CAS1*, which is required for O-  
163 acetylation, results in a hypervirulent phenotype (41). We analyzed the same  
164 conditioned media as in **Figure 1**, but used the mAb 1326 to detect GXM. MAb 1326  
165 recognizes O-acetyl (+) GXM, but is unable to recognize O-acetyl (-) GXM. F12D2, on  
166 the other hand, recognizes both O-acetyl (+) and (-) GXM. Thus, 1326 staining intensity  
167 relative to F12D2 intensity reflects the relative proportion of O-acetyl (+) GXM present in  
168 the supernatant. We observed that 1326 staining relative to F12D2 staining increased  
169 under certain capsule inducing conditions (low nitrogen, low iron, and 10%  
170 Sabouraud's, pH 5-6), indicative of increased O-acetyl (+) GXM (**Fig. S1**). These results  
171 demonstrate that environmental conditions may also influence GXM modification,  
172 specifically O-acetylation, with potential implications for immune recognition.

173

174 Identification of gene deletion mutants with reduced exo-GXM secretion under non-  
175 capsule inducing conditions.

176 We then identified mutants with reduced GXM production. We screened the *C.*  
177 *neoformans* partial knockout collection (CM18 background, 1200 targeted gene  
178 knockouts) (42) under YNB, which results in high exo-GXM production. We grew each  
179 strain for 24 hours at 37°C, removed the cells by centrifugation, then probed the  
180 conditioned medium for exo-GXM.

181 We searched the YNB-grown mutants for samples that produced less exo-GXM  
182 than wild-type cells. We then stained induced cell surface capsule (by growth in 10%  
183 Sabouraud's, pH 7.3) in this subset of mutants and eliminated any with a growth defect

184 and/or a substantial reduction (>25%) reduction in cell surface capsule thickness. We  
185 also stained for common pathogen-associated molecular patterns (PAMPs), such as  
186 exposed mannoproteins and chitin, which activate host immune responses (43). This  
187 left us with a single mutant, *cnag\_06464Δ*, or *liv7Δ*, which we re-constructed in the  
188 KN99 genetic background (**Fig. 2**). Four other mutants (**Table S1**) exhibited a moderate  
189 defect in cell surface capsule in addition to their moderate defects in exo-GXM release.  
190 However, we focused on the *liv7Δ* mutant because of its ability to form wild-type levels  
191 of cell surface capsule.

192 The *LIV7* gene was previously identified in a screen for mutants deficient in  
193 growth in the lung (42). *Liv7* is localized to the Golgi under capsule-inducing conditions  
194 (DMEM + 5% CO<sub>2</sub>) (44). *liv7Δ* cells produce wild-type-like levels of cell surface capsule  
195 when grown in 10% Sabouraud's, pH 7.3 (**Fig. 2A,B**), but conditioned medium from  
196 *liv7Δ* cell cultures grown in YNB contains two-fold less GXM than conditioned medium  
197 from wild-type *C. neoformans* cell cultures (**Fig. 2C,D**). PAMP exposure is comparable  
198 to wild-type cells (**Fig. S2**).

199

200 Identification of gene deletion mutants with elevated exo-GXM secretion under strong  
201 capsule inducing conditions.

202 We next identified mutants that produced elevated levels of exo-GXM under  
203 capsule-inducing conditions, when exo-GXM production is very low. We again screened  
204 the *C. neoformans* knockout mutant collection (CM18 background), this time growing  
205 the mutants in YNB, then subculturing by diluting 1:100 into 10% Sabouraud's, pH 7.3,  
206 and growing 48 hours at 37°C. We again removed mutants that exhibited growth

207 defects, elevated PAMP exposure, and a substantial reduction (>25%) reduction in cell  
208 surface capsule thickness. We found two groups of mutants: group #1 exhibited  
209 approximately wild-type capsule thickness, while group #2 mutants had less-than-wild-  
210 type levels of cell surface capsule (**Table S1**). We focused our subsequent experiments  
211 on the mutant in gene *cnag\_00658*, which produces cell surface capsule with the same  
212 thickness as wild-type cells (**Fig. 3A,B**). As with *l/v7Δ*, we re-constructed this mutant in  
213 the KN99 genetic background and used those strains for all subsequent experiments.  
214 As in the CM18 background, *cnag\_00658Δ* cells in the KN99 background released  
215 increased exo-GXM in 10% Sabouraud's, pH 7.3 (**Fig 3C,D**). Unlike other mutants in  
216 group #1, *cnag\_00658Δ* cells produce the same levels of melanin and urease as wild-  
217 type cells (**Fig. S2**).

218 The *CNAG\_00658* gene encodes a predicted protein 624aa in length. It shares  
219 N-terminal sequence homology with the *Schizosaccharomyces pombe* inner nuclear  
220 membrane protein, IMA1 (615aa). *CNAG\_00658*'s predicted gene product also has five  
221 putative transmembrane domains that positionally align with the 5 transmembrane  
222 domains of the *S. pombe* IMA1 protein. For these reasons, we propose to rename the  
223 *CNAG\_00658* gene, "*IMA1*". For the duration of this text, we will refer to "*cnag\_00658*"  
224 as "*ima1*".

225

226 *Changes in exo-GXM levels alter fungal cell adherence.*

227 We had thus far only assayed exo-GXM secretion during planktonic growth.  
228 However, within its natural environment of soil and vegetable matter, *C. neoformans*  
229 can form adherent biofilms (45). Previous work on cryptococcal biofilms has revealed

230 that a significant portion of the extracellular matrix is composed of GXM, and that it  
231 plays a critical role in adherence (46). Acapsular strains are unable to adhere to  
232 surfaces such as polystyrene, and the addition of anti-GXM antibodies to developing  
233 wild-type biofilms reduces their adherence (46). We speculated that exo-GXM may be  
234 incorporated into the extracellular matrix during sessile growth to provide community  
235 level structure, and that our exo-GXM mutants would display varying adherence  
236 corresponding to their exo-GXM secretion profiles.

237 To test this, we grew cells at a concentration of  $10^6$  cells/100ul in 96 well  
238 polystyrene plates at 37°C. After 48 hours, the wells were washed forcefully with  
239 PBS+0.1% tween-20 dispensed from an automated plate washer, resuspended in PBS  
240 containing XTT/menadione and left for 5 hours at 37°C. XTT is reduced by fungal cells  
241 to produce a colorimetric measure of metabolism that is highly correlative with viable  
242 cell count (47).

243 Wild-type, *cap60Δ*, *liv7Δ#1 / #2*, and *ima1Δ#1 / #2* cells were assayed in both  
244 YNB and 10% Sabouraud's pH 7.3 to replicate planktonic non-capsule and capsule-  
245 inducing conditions respectively. The *cap60Δ* cells served as a negative control, as  
246 acapsular mutants are unable to adhere, likely due to their lack of surface and exo-GXM  
247 (46). We hypothesized that *liv7Δ#1 / #2* cells would display reduced adherence in our  
248 assay due to the reduction in exo-GXM release we observed during planktonic growth.  
249 This was indeed the case, as we observed an approximately two-fold reduction in the  
250 ability of *liv7Δ#1 / #2* cells to adhere in our assay (**Fig. 4A**).

251 In contrast to YNB, *liv7Δ#1 / #2* cells were able to adhere at wild-type levels  
252 when grown in 10% Sabouraud's pH 7.3, perhaps because our observations of

253 planktonic cells indicated that far less exo-GXM is released by both wild-type and  
254 *liv7Δ#1 / #2* cells under these conditions (**Fig 4B**). Similarly, *ima1Δ#1 / #2* cells, which  
255 displayed elevated exo-GXM secretion under strong capsule inducing conditions,  
256 demonstrated six to eight-fold higher adherence than wild-type when grown in 10%  
257 Sabouraud's pH 7.3 (**Fig 4B**). When grown in YNB, *ima1Δ#1 / #2* cells still displayed  
258 increased adherence, but it was reduced to an approximately two-fold increase over  
259 wild-type (**Fig 4A**). Altogether, these results suggest that the regulated secretion of exo-  
260 GXM may have a specialized role in an environmental setting by promoting the  
261 adherence of *C. neoformans* communities.

262

263 Host survival and fungal burden correlates with *in vitro* exo-GXM levels.

264 Next, we sought to use *liv7Δ#1 / #2* and *ima1Δ#1 / #2* as an opportunity to  
265 explore roles for exo-GXM during pathogenesis. We hypothesized that exo-GXM  
266 secretion would promote virulence through its immunomodulatory properties. Since  
267 *liv7Δ#1 / #2* and *ima1Δ#1 / #2* cells produce wild-type sized surface capsules in culture,  
268 we anticipated that *liv7Δ#1 / #2* and *ima1Δ#1 / #2* cells would allow us to assess the  
269 role of exo-GXM in pathogenesis, independent of surface capsule. We predicted that  
270 the reduction of *liv7Δ#1 / #2* cells' ability to produce exo-GXM *in vitro* would result in  
271 reduced virulence. Similarly, we predicted that *ima1Δ#1 / #2* cells, which show  
272 increased exo-GXM under capsule inducing conditions, would display heightened  
273 virulence.

274 We employed a murine model of disseminated cryptococcosis by inoculating  
275 C57BL/6NJ mice (Jackson Labs) intranasally with  $2.5 \times 10^4$  fungal cells per mouse. We

276 calculated survival as the time it took each mouse to reach 85% of their initial mass.  
277 Consistent with our hypothesis, *in vitro* exo-GXM production inversely correlated with  
278 host-survival. Wild-type KN99 infected mice reached endpoint a median of 20 days  
279 post-inoculation (dpi). In contrast, *liv7Δ#1 / #2*-infected mice reached endpoint a median  
280 of 22.5 dpi, and *ima1Δ#1 / #2*-infected mice a median of 18 dpi (**Fig. 5A**). However, it is  
281 important to note that all strains were sufficiently virulent to cause lethal infection at our  
282 inoculating dose. This was not altogether unexpected, as the exo-GXM secretion  
283 phenotypes for *liv7Δ#1 / #2* and *ima1Δ#1 / #2* cells were dependent on growth  
284 conditions, and manifested as a gradient of exo-GXM production rather than complete  
285 ablation or overexpression.

286 We also assessed fungal burden by plating homogenized organs for colony  
287 forming unit (CFU) counts. Organ fungal burden followed the same trends as survival.  
288 Mice inoculated with *liv7Δ#1 / #2* cells consistently presented with lower fungal burden  
289 in the lungs by day 10 post-inoculation (**Fig. 5B**). Dissemination of *liv7Δ#1 / #2* cells to  
290 the spleen (**Fig. S3**) and brain (**Fig. 5C**) was also reduced compared to wild-type. In  
291 contrast, mice inoculated with *ima1Δ#1 / #2* cells suffered higher pulmonary fungal  
292 burden compared to those inoculated with wild-type *C. neoformans* (**Fig. 5D**).  
293 Differences were present as soon as 3 days post-inoculation (**Fig. 5D**). We also  
294 observed a greater number of disseminated *ima1Δ#1 / #2* cells in the liver and spleen  
295 throughout the course of infection (**Fig. S3**). *ima1Δ#1 / #2* cells disseminated to the  
296 brain earlier than wild-type cells, with some *ima1Δ#1 / #2* infected mice showing CFUs  
297 in the brain as early as 3 dpi (**Fig 5E**). Total brain fungal burden in *ima1Δ#1 / #2*  
298 infected mice trended higher than wild-type, with one independent gene deletion strain

299 achieving a statistically significant increase in fungal burden 10 dpi and beyond, despite  
300 high variance in dissemination at the observed time points (**Fig. 5E**). These results  
301 suggest that time-to-endpoint for the mice was at least partially due to fungal lung  
302 burden and extrapulmonary dissemination, both of which correlated with *in vitro* exo-  
303 GXM secretion.

304 Since *in vitro* exo-GXM production by *ima1Δ#1 / #2* and *liv7Δ#1 / #2* cells  
305 correlated with virulence *in vivo*, we examined whether or not the *in vitro* phenotypes  
306 would translate to detectable differences in exo-GXM production in the host  
307 environment. We analyzed the levels of GXM in the lungs, livers, spleens and brains of  
308 infected mice by performing GXM ELISA's on 0.22  $\mu$ m filtered organ homogenates.  
309 Exo-GXM levels *in vivo* were highly variable, perhaps reflecting the heterogeneous host  
310 environment or assay insensitivity (**Fig. S4**). In spite of this variability, we detected  
311 significant reductions in total exo-GXM in the lungs and extrapulmonary organs of  
312 *liv7Δ#1 / #2* infected mice at certain time points, with these trends becoming more  
313 apparent as infection progressed (**Fig. S4A-D**). Similarly, *ima1Δ#1 / #2* infected mice  
314 displayed increased total exo-GXM in the lungs, spleen and liver by 14 dpi (**Fig. S4E-G**). We did not observe any interpretable differences in exo-GXM levels on a per cell  
315 basis (data not shown), possibly due to changing host conditions over the course of  
316 dissemination or assay variability. Spread and/or clearance of exo-GXM within the host  
317 likely also played a role, as the spleen and livers of infected mice had massively  
318 increased exo-GXM levels on a per cell basis.

320 Also of note, is that we detected exo-GXM in extrapulmonary organs prior to  
321 consistent detection of colony forming units (CFU) in those same organs (**Fig. S5**). This

322 observation may be relevant for diagnosticians interested in detecting cryptococcal  
323 infection prior to dissemination in at-risk patient populations, as early diagnosis of  
324 cryptococcosis greatly improves outcomes (48).

325

326 Cell size shifts dramatically during the course of infection parallel to increases in exo-  
327 GXM.

328 We investigated whether or not *in vitro* capsule phenotypes for the mutants were  
329 recapitulated *in vivo*. We isolated cryptococcal cells from infected mice, fixed them with  
330 paraformaldehyde, and measured cell body diameter, cell surface capsule thickness,  
331 and total diameter (cell diameter including capsule) using india ink (**Fig. 1A**).

332 In wild-type-infected mice, cell and capsule size in the lungs was a broad  
333 distribution that shifted significantly over the course of infection, as observed by others  
334 (49-51). Large cells were in high abundance early in infection, particularly at 3 dpi (**Fig.**  
335 **6A**). These cells were likely Titan cells, which are large, highly polyploid, and increase  
336 their size and ploidy through non-mitotic genome replication (14). However, as infection  
337 progressed, the frequency of large cells decreased. By 20 dpi, smaller cells around  
338 10µm in total diameter dominated the lungs in number (**Fig. 6A**). The cell body size and  
339 capsule thickness distributions experienced proportional shifts, such that overall cell  
340 size to capsule thickness ratios were maintained (**Fig. S6A,B**). In the brain, the  
341 distribution of cell and capsule size was much narrower and overlapped with the  
342 population of smaller cells in the lungs (**Fig. 6B**).

343 When we compared the total cell diameter distributions of wild-type and the exo-  
344 GXM mutants in the lungs, there was no difference 3 dpi (**Fig. 6C,D**). By an early time

345 point in dissemination (14 dpi), however, the frequency of smaller cells was higher in  
346 *ima1Δ#1 / #2* infected mice and lower in *l/lv7Δ#1 / #2* infected mice, when compared to  
347 wild-type (**Fig. 6E,F**). The ratio of cell size to capsule thickness was similar amongst all  
348 strains (**Fig. S6C**).

349 Due to this correlation between cell and capsule size and exo-GXM, we  
350 hypothesized that levels of exo-GXM could influence cell and capsule size. To test this,  
351 we grew cells in strong cell surface capsule-inducing medium (10% Sabouraud's, pH  
352 7.3) with minimal exo-GXM release. After 24 hours growth at 37°C, we diluted the  
353 cultures 1:2 in fresh medium and added 100 ng/ml, 10 µg/ml, or 50 µg/ml of purified  
354 GXM. After an additional 24 hours growth, we measured cell and capsule size. We  
355 found that both capsule thickness (**Fig. 7A**) and cell size (**Fig. S7A**) decreased in a  
356 dosage-dependent manner. The greatest decrease was in capsule thickness, which  
357 showed a decrease from a median of 4 µm in control cultures to 1.5 µm in cultures  
358 treated with 50 µg/ml GXM, a decrease of 62.5%. 100 ng/ml showed a more modest  
359 decrease, to a median capsule thickness of 3.6 µm (a 10% decrease). 50 µg/ml and 10  
360 µg/ml GXM treatments also resulted in a change in cell size, from a median of 6.0 µm  
361 for untreated cells to 4.5 µm and 5.3 µm, respectively. 100 ng/ml GXM did not result in a  
362 decrease in cell size, despite the observed change in capsule thickness (**Fig. S7A**).

363 GXM purification can result in contamination by detergents from the purification  
364 protocol (30). Thus, we performed the same experiment, but added conditioned medium  
365 (from a YNB-grown culture) instead of purified GXM. 20%, 10%, or 1% final  
366 concentration of conditioned medium resulted in decreases in both capsule thickness  
367 and cell size (**Fig. 7B, Fig. S7**). These capsule and cell size changes also depended on

368 growth: if we did not add fresh medium along with purified GXM, capsule thickness and  
369 cell size did not change (**Fig. S7**).

370 Altogether, these data suggest that changes to exo-GXM observed *in vitro* can  
371 affect pathogenesis. Total exo-GXM secreted throughout infection correlated with  
372 decreased survival, increased fungal burden and more rapid generation of smaller  
373 (haploid) cells in the lungs, which appear more likely to disseminate due to their  
374 dominant presence in extrapulmonary organs.

375

376 Exo-GXM limits innate immune cell infiltration into the brain.

377 In human patients, cryptococcal meningoencephalitis is associated with a striking  
378 paucity of inflammation (9). The main driver of mortality, particularly in  
379 immunocompromised patients, is thought to be excessive fungal burden and GXM  
380 accumulation within the CNS, which leads to a devastating increase in intracranial  
381 pressure (10). C57BL/6NJ mice infected with the highly virulent KN99 strain display a  
382 similar paucity of brain inflammation, despite significant fungal presence. For instance,  
383 when we histologically compared the brains of KN99 infected mice to mock-infected  
384 animals, we could detect very little sign of infiltrating immune cells by H&E staining in  
385 KN99-infected mice, despite local presence of fungi (**Fig. S8**). This was true both early  
386 (14 dpi) (**Fig. S8A,B**) and late (21 dpi) in disseminated infection (**Fig. S8C,D**).  
387 Considering its immunosuppressive nature, we hypothesized that GXM could very likely  
388 play a role in limiting brain inflammation during infection. We correspondingly reasoned  
389 that infection with *liv7Δ#1 / #2* cells might result in increased immune infiltration into the  
390 brain, due to *liv7Δ#1 / #2* cell's reduced exo-GXM secretion.

391 In order to address this hypothesis, we harvested the brains of wild-type and  
392 *liv7Δ#1 / #2* infected animals at 20 days post-intranasal inoculation and analyzed  
393 immune infiltration into the brain via flow cytometry. CD4+ (**Fig. 8A**) and CD8+ (**Fig. 8B**)  
394 cells were scarce in both wild-type and *liv7Δ#1 / #2*-infected brains. These data suggest  
395 that T cells do not significantly respond to brain invasion by *C. neoformans*. Innate  
396 immune cells (macrophages/neutrophils) did show some response to wild-type *C.*  
397 *neoformans* cells in the brain, but it was only slightly elevated when compared to mock-  
398 infected animals (**Fig. 8C,D**). This is in stark contrast to bacterial or viral meningitis,  
399 which often show high levels of infiltrating neutrophils and macrophages (7, 8).  
400 Infiltration of both macrophages and neutrophils was increased in *liv7Δ#1 / #2* infected  
401 brains (**Fig. 8C,D**). These results suggest that exo-GXM likely plays an important role in  
402 brain immunosuppression that is independent of surface capsule.

403 We next sought to determine if exo-GXM was sufficient to suppress immune  
404 infiltration into the brain if we induced brain inflammation by direct intracranial  
405 inoculation. We purified GXM from YNB-grown cultures using standard methods (30).  
406 Since we detected GXM associated with the brain up to five days prior to the  
407 appearance of CFU (**Fig. S5**), we administered 200 µg of purified GXM daily by  
408 intraperitoneal injection, beginning five days prior to inoculation (**Fig. 9A**). Additional  
409 mice were administered sterile PBS as a control. We then inoculated mice intracranially  
410 with either wild-type KN99 or acapsular *cap60Δ* cells. Unsurprisingly, *cap60Δ* cells  
411 elicited greater numbers of immune infiltration into the brain (**Fig. 9B,C**), and achieved a  
412 significantly lower fungal burden than wild-type *C. neoformans* (**Fig. 9D**). However,  
413 administration of GXM to mice infected with *cap60Δ* cells reduced immune infiltration

414 (CD45<sup>hi</sup> cells) into the brain (**Fig. 9B,C and Fig. S9**), and increased fungal burden when  
415 compared to PBS-treated mice (**Fig. 9D**). These results demonstrate that in the context  
416 of an inflammatory infection, exo-GXM is sufficient to promote fungal survival in the  
417 brain, likely through the suppression of brain immune infiltration.

418

419 **Discussion:**

420 Surface capsule is critical for *C. neoformans* virulence. However, GXM that is not  
421 attached to the cell surface, or exo-GXM, accumulates to significant levels in laboratory  
422 culture and during infection (10, 30, 31). Our data strongly suggest that *C. neoformans*  
423 inversely regulates surface capsule formation and exo-GXM release according to  
424 environmental cues. Within our tested conditions, GXM was constitutively produced but  
425 alternately retained at the cell surface or released into the extracellular milieu. Previous  
426 findings have also indicated that exo-GXM release might be an active process. For  
427 instance, a study comparing the properties of exo-GXM and capsular GXM showed that  
428 despite sugar composition remaining the same, capsular GXM and exo-GXM  
429 manifested distinct biophysical and antigenic properties (34). Additionally,  
430 electromobility of exo-GXM decreases under capsule inducing conditions, implying that  
431 structural changes that influence capsule formation (35). We also observed that O-  
432 acetylation of GXM's mannose backbone changes with environmental conditions. These  
433 findings potentially suggest that differential regulation of surface capsule and exo-GXM  
434 could occur at the level of GXM polymer length and/or other modification. More work is  
435 required to elucidate biophysical differences between cell surface retained- and exo-  
436 GXM.

437            We identified genes that play a role in exo-GXM release. Deletion of *LIV7*  
438    reduces exo-GXM release in rich growth medium when cell surface capsule does not  
439    form, but does not affect capsule thickness. It has been previously demonstrated that  
440    *LIV7* is important for virulence and likely functions in Golgi transport (42, 44). Our  
441    second exo-GXM mutant, a deletion of the gene *IMA1*, increased exo-GXM release  
442    under strong capsule inducing conditions without affecting capsule thickness. We used  
443    these two exo-GXM mutants as tools to investigate the biological importance of exo-  
444    GXM independent of surface capsule.

445            We first established a positive correlation of exo-GXM release with biofilm  
446    adherence, suggesting that exo-GXM release during environmental growth may be  
447    important for promoting community level structure and adherence. It would not be  
448    surprising for there to be additional functions for exo-GXM in environmental settings.

449            In a murine infection model, we showed a correlation between elevated *in vitro*  
450    exo-GXM levels, fungal burden and poor host survival. Other groups have also  
451    connected varied exo-GXM release with changes to virulence. Analysis of a virulence-  
452    associated transcriptional network map previously revealed a positive correlation with  
453    exo-GXM release and mouse lung infectivity over 7 days (52). However, the  
454    transcription factor mutants also had altered surface capsule thickness, which may have  
455    influenced infectivity (52). Deletion of the flippase encoding gene *APT1* also resulted in  
456    reduced *in vitro* exo-GXM release despite wild-type surface capsule. The knockout was  
457    hypovirulent, but in contrast to our mutants, had reduced surface capsule thickness *in*  
458    *vivo* (53). Our results support these previous findings, and our new exo-GXM mutants  
459    are a powerful tool for investigating exo-GXM because they do not suffer any alterations

460 to additional virulence factors. Our data also provide additional support for a model in  
461 which regulated release of exo-GXM enhances virulence independent of surface  
462 capsule.

463 Interestingly, exo-GXM also correlated with changes in cell body and capsule  
464 size distributions in the lungs. In wild-type *C. neoformans* infected animals, fungal cell  
465 body size and capsule thickness decreased over the course of infection, as exo-GXM  
466 levels increased. Correspondingly, increased GXM levels in the mouse lungs positively  
467 correlated with an increased frequency of smaller cells at an early time point in  
468 dissemination. *C. neoformans* cells in the brain and other extrapulmonary organs are  
469 much smaller than the lungs (**Fig. 6B** and (50, 54, 55)), suggesting that the emergence  
470 of smaller cells in the lungs is an important step in dissemination. The addition of  
471 purified GXM to *C. neoformans* cells growing in capsule-inducing media was sufficient  
472 to decrease cell body size and capsule thickness in a growth-dependent manner (**Fig.**  
473 **7**). These data suggest that exo-GXM may actually provide a concentration-dependent  
474 signal to *C. neoformans* cells that reduces cell size and capsule thickness. In the lungs,  
475 this mechanism may be a contributing factor in the generation of small cells with a  
476 greater propensity for dissemination.

477 There is large body of literature demonstrating immunosuppressive properties for  
478 GXM (19). We focused on the brain, as cryptococcal meningoencephalitis is the leading  
479 cause of death in cryptococcosis patients and is characterized by low levels of  
480 inflammation (9). Here, we observed that deleting a gene required for wild-type levels of  
481 exo-GXM release *in vitro* (*lIV7*) altered the host immune response to *C. neoformans*  
482 brain infection. Mice infected with *lIV7*Δ cells had increased macrophages and

483 neutrophils infiltrating the brain, compared to wild-type infected mice. Furthermore,  
484 administration of purified GXM was sufficient to reduce brain infiltrating immune cells in  
485 the context of acapsular *C. neoformans* infection. These data echo a previous study that  
486 showed GXM could reduce early infiltration of neutrophils in a model of acute bacterial  
487 meningitis (56). Our results suggest that exo-GXM is an actively secreted virulence  
488 factor that may influence cell morphology to facilitate dissemination, and is capable of  
489 distally suppressing immune infiltration into the brain.

490

491 **Funding information**

492 This work was supported by a startup grant from the Pathology Department at the  
493 University of Utah to J.C.S.B. and NIH R01 NS041249 to T.E.L.

494

495 **Figure 1: Levels of detectable exo-GXM negatively correlate with capsule**  
496 **thickness under a variety of media conditions.** To generate conditioned media, we  
497 normalized 24 hour cultures by volume, then passed the supernatants through a 0.22  
498  $\mu\text{m}$  filter to remove fungal cells. **(A)** Representative image of cell/capsule  
499 measurements used in this study. **(B)** We tested supernatants for free GXM (“exo-  
500 GXM”) by blotting and probing with the F12D2 anti-GXM mAb. See Materials and  
501 Methods for further details. A representative blot showing relative levels of exo-GXM  
502 collected from cells cultured for 24 hours under a variety of capsule and non-capsule  
503 inducing conditions. **(C)** Intensity of exo-GXM bands relative to YNB+2% glucose exo-  
504 GXM (blue bars) were quantitated for three independent experiments and plotted next  
505 to absolute measurements of capsule thickness (yellow bars) (n=30 cells). Data was

506 combined from three independent experiments. Bars represent the mean and error bars  
507 represent the standard deviation (SD).

508

509 **Figure 2: Identification of a genetic mutant (*liv7Δ*) with reduced exo-GXM release,**  
510 **but no observable changes to capsule thickness.** (A) Representative india ink  
511 images of cells grown in 10% Sabouraud's dextrose pH 7.3 for 24 hours. Capsule  
512 thickness was similar across KN99 wild-type (WT) cells, and cells from each  
513 independent *liv7* deletion strain (*liv7Δ#1* and *liv7Δ#2*) (B) Quantification of cell body  
514 diameter and capsule thickness from three independent experiments (n=30 cells per  
515 strain; bars represent mean with SD). (C) Conditioned media from wild-type and mutant  
516 cultures grown in weak-capsule inducing conditions (YNB + 2% glucose) for 24 hours.  
517 Blots were probed with anti-GXM antibody F12D2. (D) Quantification of blot signal  
518 intensities shows reduced exo-GXM release by *liv7Δ#1* / *liv7Δ#2*. Data was combined  
519 from three independent experiments. P-values were calculated using a Mann-Whitney  
520 test; bars represent mean with SD.

521

522 **Figure 3: Identification of a genetic mutant (*ima1Δ*) with increased exo-GXM**  
523 **release, but no observable changes to capsule thickness.** (A) Representative india  
524 ink images of cells grown in 10% Sabouraud's dextrose pH 7.3 for 24 hours. Capsule  
525 thickness was similar across KN99 wild-type (WT) cells, and cells from each  
526 independent *ima1* (also *cnag\_00658*, see main text for details) deletion strain (*ima1Δ#1*  
527 and *ima1Δ#2*). (B) Quantification of cell body diameter and capsule thickness from three  
528 independent experiments (n=30 cells per strain; bars represent mean with SD) (C)

529 Conditioned media from cultures grown for 24 hours under strong capsule-inducing  
530 conditions (10% Sabouraud's at pH 7.3). Blots were probed with anti-GXM antibody  
531 F12D2. **(D)** Quantification of blot signal intensities shows increased exo-GXM release  
532 by *ima1Δ#1 / ima1Δ#2* (Combined data from three independent experiments. P-values  
533 were calculated using a Mann-Whitney test; bars represent mean with SD.

534

535 **Figure 4: Mutants' alterations to exo-GXM release correlates with adherence.**  $10^6$   
536 *C. neoformans* cells were seeded into individual wells of 96-well polystyrene plates and  
537 incubated at 37°C. 48 hours later, the wells were washed to remove non-adhered  
538 and/or weakly adhered cells before resuspension in XTT for colorimetric analysis of  
539 metabolic activity as a proxy for viable cell count. **(A)** OD<sub>490</sub> readings from cells grown in  
540 YNB, normalizing to wild-type cell readings. *liv7Δ#1 / #2* cell adherence was reduced  
541 and *ima1Δ#1 / #2* cell adherence was increased when compared to wild-type cells. **(B)**  
542 OD<sub>490</sub> readings from cells grown in 10% Sabouraud's pH7.3, normalizing to wild-type  
543 cell readings. *ima1Δ#1 / #2* cell adherence was increased when compared to wild-type  
544 cells. Combined data from three independent experiments. P-values were calculated  
545 using a Mann-Whitney test; bars represent mean with SD.

546

547 **Figure 5: Mutants' alterations to *in vitro* exo-GXM release correlate with changes**  
548 **in survival and fungal burden during infection.** **(A)** C57BL/6NJ mice infected  
549 intranasally with *ima1Δ#1 / #2* (n=10 and n=10, respectively) reach endpoint  
550 significantly sooner than wild-type infected mice (n=15). Wild-type infected mice  
551 reached endpoint sooner than *liv7Δ#1 / #2* (n=8 and n=14, respectively) infected mice.

552 Mock infected animals given sterile 1X PBS (n=5) did not show signs of disease 35  
553 days post-inoculation. P-values were calculated using a Log-rank (Mantel-Cox) Test. **(B**  
554 **and C)** Lung fungal burden is significantly higher in *ima1Δ#1 / #2* (n=8 and n=8,  
555 respectively) infected mice than wild-type infected mice (n=8) beginning at least 3 days  
556 post-inoculation, while *liv7Δ#1 / #2* infected mice (n=8 and n=8, respectively) show  
557 decreased lung burden beginning between 10 days post-inoculation compared to wild-  
558 type (n=12). **(D and E)** Dissemination to the brain trends higher in *ima1Δ#1 / #2* infected  
559 mice, and is significantly lower in *liv7Δ#1 / #2* infected animals when compared to wild-  
560 type P-values were calculated using a Mann-Whitney test.

561

562 **Figure 6: Cell size distributions over the course of infection.** We visualized fungal  
563 cells from tissue homogenates (from infected mice in **Fig. 5B-E**) in india ink and  
564 measured cell surface capsule size. Total diameter = cell + capsule diameter. Cell body  
565 diameter = diameter from one edge of the cell wall to the other. Capsule thickness =  
566 (total diameter -- cell body diameter)/2 (**Fig 1A**). **(A)** Mean total cell diameter decreases  
567 over time within the lungs of wild-type infected mice as the population shifts toward  
568 smaller cells with smaller capsules (n=3-4 mice per time point,  $\geq 120$  cells per mouse).  
569 **(B)** Disseminated cells found in the brain late in infection (20 dpi) overlay with the size  
570 profile of smaller cells found in the lungs at the same time point. **(C and D)** Early after  
571 inoculation (3 dpi) the distributions of both **(C)** *liv7Δ#1 / #2* and **(D)** *ima1Δ#1 / #2* cells  
572 match that of wild-type in the lungs (n=3 mice,  $\geq 50$  cells per mouse). **(E and F)** At an  
573 early point in dissemination (14 dpi), **(E)** *liv7Δ#1 / #2* cell populations were of larger  
574 average total cell diameter than wild-type *C. neoformans* cells in the lungs. **(F)** *ima1Δ#1*

575 / #2 cells were of smaller average total cell diameter than wild-type *C. neoformans* cells  
576 (n=4 mice,  $\geq$ 120 cells per mouse). P-values were calculated using a Mann-Whitney test.

577

578 **Figure 7: Treatment with GXM decreases capsule thickness.** We induced cell  
579 surface capsule by growing cells 24 hours in 10% Sabouraud's pH 7.3, then added  
580 various concentrations of either (A) purified GXM or (B) conditioned medium from a  
581 YNB-grown culture of wild-type (KN99) *C. neoformans* cells. We find a dosage-  
582 dependent decrease in capsule thickness following exposure to both purified GXM and  
583 conditioned medium. Histograms contain data from four separate experiments, with at  
584 least 60 cells measured per condition for each experiment. We also observed a  
585 decrease in cell size (see **Fig. S7**) with GXM or conditioned medium treatment. P-  
586 values were calculated using a Mann-Whitney test. Representative DIC images of (C)  
587 untreated cells or (D) cells treated with 50  $\mu$ g/ml GXM are shown.

588

589 **Figure 8: Mice infected with *liv7Δ* cells display increased innate immune infiltrate**  
590 **in the brain.** Mouse brains were harvested late (20 dpi) in infection for flow cytometry  
591 analysis of infiltrating immune cells. (A) CD4 $^{+}$  T cells are scarce in both wild-type and  
592 *liv7Δ*#1 / #2 infected brains. (B) CD8 $^{+}$  T cells show a significant increase over wild-type  
593 in *liv7Δ*#2 infected brains, but this was not replicated in *liv7Δ*#1 infected brains (C)  
594 Macrophages (CD45 $^{\text{hi}}$ F4/80 $^{+}$ ) and (D) neutrophils (CD45 $^{+}$ Ly6G $^{+}$ Ly6C $^{+}$ ) are significantly  
595 increased in the brains of *liv7Δ*#1 and #2 as compared to wild-type and mock-infected  
596 brains. P-values were calculated using a Mann-Whitney test; bars represent the  
597 median.

598

599 **Figure 9: Purified GXM is sufficient to suppress immune infiltration into the brain**

600 **in response to inflammation-inducing acapsular (*cap60* $\Delta$ ) *C. neoformans*.** 6-week-

601 old C57Bl/6NJ mice were intracranially inoculated with 200 *cap60* $\Delta$  fungal cells in 30  $\mu$ l

602 1X PBS. Beginning 5 days prior to inoculation, mice were administered intraperitoneal

603 injections of either 200  $\mu$ g/mL GXM or 200  $\mu$ l sterile PBS. On the day of inoculation,

604 mice were administered this treatment intravenously to ensure GXM would be present

605 in the blood-stream. At 3 dpi brains were harvested to determine fungal burden by

606 colony forming unit counts. Separate mice were sacrificed to analyze infiltrating immune

607 cells by flow cytometry. **(A)** Diagram of experimental procedures. **(B)** Mice infected with

608 *cap60* $\Delta$  displayed increased brain immune infiltrate (CD45 $^{hi}$  cells) over wild-type

609 infected mice. Immune infiltration into the brains of *cap60* $\Delta$  infected mice was reduced

610 with the administration of GXM. **(C)** Representative flow plots for data shown in **(B)**. **(D)**

611 Mice infected with wild-type KN99 cells suffered increased fungal brain burden as

612 compared to mice infected with *cap60* $\Delta$ . Administration of GXM had no significant effect

613 on wild-type fungal burden, but resulted in significantly increased *cap60* $\Delta$  fungal burden

614 compared to *cap60* $\Delta$ -infected mice that did not receive GXM. P-values were calculated

615 using a Mann-Whitney test; bars represent the median.

616

617 **Table S1: Exo-GXM mutant screen results.** We screened the *C. neoformans* partial

618 knockout collection (CM18 background, 1200 targeted gene knockouts) under YNB,

619 which results in high exo-GXM release by wild-type cells, or 10% Sabouraud's pH7.3,

620 which results in low exo-GXM release. **(A)** Gene deletions which resulted in reduced

621 exo-GXM release in YNB after 24 hours but no growth defect or a substantial reduction  
622 (>25%) reduction in cell surface capsule thickness in 10% Sabouraud's pH 7.3. **(B)**  
623 Gene deletions which resulted in increased exo-GXM release in 10% Sabouraud's pH  
624 7.3 after 24 hours. Class 1 gene deletion mutants had approximately wild-type-sized  
625 capsule thickness, while Class 2 mutants had reduced capsule thickness in 10%  
626 Sabouraud's pH 7.3.

627

628 **Figure S1: Proportion of O-acetylated exo-GXM increases under stronger capsule**  
629 **inducing conditions.** Conditioned media was collected and blotted as in **Fig. 1. (A)**  
630 Detection of GXM with an acetylation insensitive mAb (F12D2). **(B)** Detection of GXM  
631 from the same conditioned media with an acetylation-sensitive mAb (1326), which only  
632 recognizes O-acetylated GXM. Increased intensity indicates a greater level of O-  
633 acetylated GXM.

634

635 **Figure S2: Canonical virulence determinants are intact in *liv7Δ* and *ima1Δ* cells.**  
636 **(A)** Cells were grown overnight in YNB + 2%glucose, stained with the fluorescently  
637 labeled lectins concanavalin A (ConA-rhodamine) and wheat germ agglutinin (WGA-  
638 fluorescein) to estimate exposure of PAMPs on the cell surface. **(B)** Cells were grown  
639 overnight in YNB + 2%glucose, subcultured 1:100 in 10% Sabouraud's dextrose (10%  
640 sab), pH 7.3, and stained as in **(A)**. PAMP exposure was similar across all strains  
641 except *cap60Δ*, which lacks surface capsule. **(C)**  $2.5 \times 10^4$  cells were spotted on L-3,4-  
642 dihydroxyphenylalanine (L-DOPA) agar to observe melanization 48 hours later. No  
643 obvious differences were detected. **(D)**  $2.5 \times 10^4$  cells were spotted on Christensen's

644 urea agar to observe urease secretion 48 hours later as the change in agar coloration  
645 from orange to pink. No obvious differences were detected.

646

647 **Figure S3: Liver and spleen fungal burden mostly correlates with *in vitro* exo-  
648 GXM production.** These data are from the same experiments as in **Fig. 5.** **(A)** Fungal  
649 burden in the livers of wild-type and *liv7Δ#1 / #2* infected mice did not show consistent  
650 differences over the course of infection. **(B)** Fungal burdens in *ima1Δ#1 / #2* infected  
651 livers were significantly higher than wild-type at 14 and 16 dpi. **(C)** Fungal burden in the  
652 spleens of *liv7Δ#1 / #2* infected mice was significantly lower than wild-type-infected  
653 mice at 10 and 17 dpi. **(D)** Fungal burdens in *ima1Δ#1 / #2*-infected spleens were  
654 significantly higher than wild-type infected mice at 14 and 16 dpi. P-values were  
655 calculated using a Mann-Whitney test.

656

657 **Figure S4: Total free GXM levels in mice infected with *C. neoformans* exo-GXM  
658 mutants.** Tissues from mice in **Fig. 3B-G** were homogenized and passed through a  
659 0.22  $\mu$ m filter to remove fungal cells, then GXM levels were measured by ELISA. **(A)**  
660 Mouse lungs infected with *liv7Δ#1 / #2* cells showed trends toward reductions in exo-  
661 GXM levels when compared to wild-type, though statistical significance is not consistent  
662 across independent gene deletions. **(B and C)** Mouse livers and spleens infected with  
663 *liv7Δ#1 / #2* cells showed reduced exo-GXM levels when compared to wild-type-infected  
664 organs at 14 dpi. **(D)** Mouse brains infected *liv7Δ#1 / #2* cells showed reduced exo-  
665 GXM when compared to wild-type at 17 dpi. **(E-G)** Exo-GXM was increased in *ima1Δ#1 /*  
666 *#2* infected lungs, livers, and spleens when compared to wild-type-infected organs at

667 14dpi. **(H)** No significant differences in exo-GXM were observed in *ima1Δ#1 / #2*  
668 infected brains when compared to wild-type-infected brains. P-values were calculated  
669 using a Mann Whitney t test.

670

671 **Figure S5: GXM appears in brains and spleens prior to the appearance of CFU.**

672 A time course of **(A)** fungal burden (CFU) and **(B)** GXM per organ following infection  
673 with wild-type *C. neoformans* shows that GXM is detectable in all organs by 3 dpi. CFU  
674 were not detectable in brains or spleens until 10 dpi. These data are the compiled wild-  
675 type infection data from **Fig. 5**, **Fig. S3**, and **Fig. S4**.

676

677 **Figure S6: Distribution of *C. neoformans* cell body diameter and cell capsule**  
678 **thickness shift over the course of lung infection:** These data are from the same  
679 experiments as **Fig. 6**. **(A)** Average *C. neoformans* cell body diameter in the lungs  
680 decreases over the course of infection (n=3-4 mice per time point,  $\geq 120$  cells per  
681 mouse). **(B)** Average capsule thickness in the lungs decreases over the course of  
682 infection at a rate similar to the change in cell body diameter (n=3-4 mice per time point,  
683  $\geq 120$  cells per mouse). **(C)** The proportion of cell size to capsule thickness in the lungs  
684 is similar across wild-type, *liv7Δ#1 / #2*, and *ima1Δ#1 / #2* cells in the lungs (n=4 mice,  
685  $\geq 120$  cells per mouse). P-values were calculated using a Mann-Whitney test; error bars  
686 show medians.

687

688 **Figure S7: Treatment with GXM decreases cell size.** These data are from the same  
689 experiments as **Fig. 7**. Cell size decreases in a dosage-dependent manner with the

690 addition of **(A)** purified GXM at 50  $\mu$ g/ml or 10  $\mu$ g/ml, but not 100 ng/ml, even though  
691 capsule thickness decreased with the addition of 100 ng/ml GXM. **(B)** Conditioned  
692 medium at final concentrations of 20%, 10%, or 1% all decrease cell size. **(C)** Cell size  
693 and **(D)** capsule thickness do not change if cultures are not administered additional  
694 growth medium (10% Sabouraud's, pH 7.3) along with purified GXM, suggesting that  
695 these size changes are growth-dependent. P-values were calculated using a Mann-  
696 Whitney test.

697

698 **Figure S8: Few immune cells infiltrate the brains of mice with disseminated**  
699 **cryptococcosis, despite high fungal burden. (A)** Representative hematoxylin and  
700 eosin (H&E) and **(B)** consecutive Grocott's methenamine silver (GMS) stained midbrain  
701 sections early (14 dpi) in brain infection. We observed no signs of inflammatory infiltrate  
702 (excess purple hematoxylin staining) and minimal fungal presence (black silver staining;  
703 arrows point to fungi) early. **(C)** Representative H&E and **(D)** GMS stained cerebral  
704 cortex sections late (21 dpi) in brain infection. We continued to detect few signs of  
705 inflammatory infiltrate in H&E stained sections late in infection, despite significant and  
706 diffuse fungal presence within the meninges and parenchyma of the brain (arrows point  
707 to fungi).

708

709 **Figure S9: Administration of purified GXM to mice inoculated intracranially with**  
710 **acapsular *C. neoformans* reduces brain immune infiltration.** These data are from  
711 the same experiments as **Fig. 10.** Brain infiltrating immune cells were detected by flow  
712 cytometry and broken into **(A)**  $CD45^{hi}F4/80^+$  macrophages, **(B)**  $CD45^+Ly6G^+Ly6C^+$

713 Neutrophils, **(C)** CD4<sup>+</sup> (T cells), **(D)** CD8<sup>+</sup> (T cells). P-values were calculated using a  
714 Mann-Whitney test.

715

716 **Methods:**

717 Conditioned media collection: *C. neoformans* cells were cultured overnight in  
718 YNB+2%glucose at 30 °C before subculturing 1:100 in the desired medium. Culture  
719 OD<sub>600</sub> readings were taken 24 hours later and were normalized to the lowest measured  
720 OD<sub>600</sub>. Cells were pelleted by centrifugation at 3000xg for 5 min. The supernatant was  
721 collected and passed through a 0.22 µm filter, yielding conditioned media.

722 The following growth media were used in this study: YPAD (20g/L bacto-peptone,  
723 10g/L bacto-yeast extract, 2% glucose, 0.4g/L adenine sulfate). YPD (20g/L bacto-  
724 peptone, 10g/L bacto-yeast extract, 2% glucose); YNB (Difco REF 291940) +2%  
725 glucose; 25% YNB+2% glucose; Low iron media (LIM) (5g/L asparagine, 0.4g/L  
726 K<sub>2</sub>HPO<sub>4</sub>, 0.1g MgSO<sub>4</sub>·7H<sub>2</sub>O, 0.5mg/L thiamine, 0.029mg/L boric acid, 1.88mg/L  
727 CuSO<sub>4</sub>·5H<sub>2</sub>O, 0.36mg/L MnCl<sub>2</sub>·4H<sub>2</sub>O, 0.021mg/L ZnCl<sub>2</sub>, 0.18mg/L NaMoO<sub>4</sub>·2H<sub>2</sub>O,  
728 0.05mg/L CaCl<sub>2</sub>·2H<sub>2</sub>O, 0.05mM bathophenanthroline disulfonic acid (BPDS), 1mM  
729 EDTA, 2% glucose, 50mM MOPS pH 6.0), 10% Sabouraud's dextrose (Difco REF  
730 238230) buffered with 50mM HEPES pH 8.0, HEPES pH 7.3, MOPS pH 6.0, or MES pH  
731 5.0; YCB (Difco REF 239110) +5g/L urea; YCB+0.5g/L urea.

732

733 Conditioned media blots: 10 µl of conditioned media collected from *C. neoformans*  
734 cultures were loaded into a 0.6% agarose gel and run at 33V for 18-20 hours at 0.5X  
735 TBE. The gels were processed with a 10 minute depurination rinse in a 0.25M HCl

736 solution, followed by a 30 minute denaturation incubation in a 1.5M NaCl/0.5M NaOH  
737 solution, and a 30 minute neutralization incubation in 1.5M NaCl/0.5M Tris-HCl, pH 7.5.  
738 The gels were rinsed in distilled water following each incubation. Gel contents were  
739 subsequently transferred to a positively charged membrane using a standard Southern  
740 blot protocol with 10X SSC (saline-sodium citrate) in the reservoir. After overnight  
741 transfer, the blots were soaked briefly in 2X SSC and dried. Blots were then blocked for  
742 1 hour in 1X PBS+5% milk and incubated shaking overnight at 4 °C in 1X PBS+5% milk  
743 with 1:40,000 anti-GXM monoclonal antibody. The following morning, blots were rinsed  
744 3 times in 1X PBS, incubated 2 hours in 1X PBS+5% milk with 1:2500 goat anti-mouse  
745 HRP antibody, and washed for 2.5 hours in 1X PBS+0.1% tween-20, changing the wash  
746 buffer every 20 minutes. For imaging, blots were developed with Clarity Western ECL  
747 substrate (BioRad Cat. 170-5061) and imaging on a BioRad Western Blot Imager. Anti-  
748 GXM monoclonal antibodies used in this study: F12D2, 1326 (Thomas Kozel, University  
749 of Nevada, Reno).

750  
751 Cell measurements: *C. neoformans* cells collected from laboratory media were spun  
752 down at 3000xg for 5 min, washed twice in 1X PBS and resuspended in 1X PBS. To  
753 collect cells from infected mouse organs, 1 mL of organ homogenate was passed  
754 through a 70 µm cell strainer (Fisher Cat. No. 22-363-548). At this junction, capsule  
755 measurement methods were the same for both laboratory-grown and mouse-isolated *C.*  
756 *neoformans* cells. Cells were fixed for 15 minutes in 2% paraformaldehyde before  
757 washing twice with 1X PBS, and resuspending in 100 µl of 1X PBS. 4 µl of cell  
758 suspension was mixed with 4 µl of india ink (Higgins No. 44201) on a microscope slide,

759 coverslipped and visualized. Successive, representative pictures were taken from the  
760 outside of the coverslipped area toward the middle, because smaller cells tended to  
761 spread towards the edges of the coverslip more so than larger cells. Total cell diameter  
762 was measured as the distance from one edge of the capsule to the opposite edge.  
763 Cell body diameter was measured as the distance from one edge of the cell wall to the  
764 opposite edge. Capsule thickness was calculated as the total cell diameter, minus the  
765 cell body diameter, and divided by two; (total cell diameter–cell body diameter)/2.

766

767 Screen for exo-GXM mutants: Cells were spotted from 96 well frozen stocks to  
768 omnitrays containing YPD agar, then grown for 48 hours at 30°C. Colonies are used to  
769 inoculate deepwell plates containing 1 ml yeast nitrogen base (YNB) per well. Deepwell  
770 plates were grown at 37°C for 48 hours with shaking (280 rpm). 10 µl of YNB culture  
771 were then used to inoculate 10% Sabouraud's (pH 7.3) cultures, which were then grown  
772 at 37°C for 48 hours with shaking. After growth, all cultures, either YNB or 10%  
773 Sabouraud's, pH 7.3, were harvested by centrifugation, then the supernatant was  
774 collected and stored for analysis.

775 We analyzed exo-GXM in YNB supernatants by dot blotting 4 µl of supernatant  
776 into each well of a dot blotter containing positively charged nylon membrane pre-soaked  
777 in 2X SSC, then applying vacuum. Membranes were air dried, then blocked and  
778 incubated with anti-GXM F12D2 antibody using standard procedures (see Materials and  
779 Methods section: *Conditioned media blots*). 10% Sabouraud's conditioned media  
780 samples were run on agarose gels and transferred to nylon membranes (see Materials  
781 and Methods section: *Conditioned media blots*).

782 Once we identified mutants with altered exo-GXM levels (decreased in YNB  
783 cultures or increased in 10% Sabouraud's, pH 7.3 cultures, we grew all mutants in 10%  
784 Sabouraud's, pH 7.3, then measured capsule thickness. Mutants with decreased cell  
785 surface capsule thickness (approximately 25% decrease compared to wild-type cells)  
786 were eliminated from further analysis. We then repeated the growth and exo-GXM blot  
787 for each strain. We normalized for cell density (to account for slow growing mutants),  
788 filtered the conditioned medium through a 0.22  $\mu$ m filter to remove cells, and ran 10  $\mu$ l  
789 of conditioned medium on an agarose gel using the procedure described in (see  
790 Materials and Methods section: *Conditioned media blots*). Finally, we stained for  
791 exposure of PAMPs such as chitin and mannosprotein (see Materials and Methods  
792 section: *Lectin Staining*) and removed mutants with increased exposure.

793

794 Lectin Staining: Cells grown for 24 hours in the appropriate media were pelleted,  
795 washed twice in 1X PBS and fixed for 12 minutes in 2% paraformaldehyde. Cells were  
796 then washed twice in 1X PBS and resuspended in 1X PBS. To an aliquot of cells, wheat  
797 germ agglutinin (WGA) conjugated to fluorescein (Vector Labs Cat. No. FL-1021) was  
798 added to a final concentration of 5  $\mu$ g/ml, and incubated 30 minutes at room  
799 temperature with shaking. At the end of the WGA incubation, concanavalin A (ConA)  
800 conjugated to rhodamine (Vector Labs Cat. No. RL-1002) was added to a final  
801 concentration of 50  $\mu$ g/ml. Cells were wash once in 1X PBS and imaged immediately.

802

803 Melanization and urease secretion: Cells grown overnight in YNB were washed twice in  
804 1X PBS and resuspended to a final concentration of  $2.5 \times 10^6$  cells/mL in 1X PBS. 10  $\mu$ l of

805 cell suspension was spotted onto L-DOPA containing agar or Christensen's urea agar  
806 (Sigma 27048). Plates were checked daily for changes in melanization (brown/black  
807 colonies on L-DOPA), and urease secretion (pink coloration surrounding colonies on  
808 Christensen's urea).

809

810 GXM purification: GXM was purified as described previously (30). Briefly, 100 mL *C.*  
811 *neoformans* cells were cultured in YNB + 2%glucose for 5 days at 30°C. Cultures were  
812 centrifuged at 12,000xg for 15min and the supernatant collected. Polysaccharides were  
813 precipitated from the supernatant overnight with the addition of 3 volumes of 95% EtOH  
814 at 4 °C. The solution was then centrifuged at 15,000xg for one hour, resuspended in  
815 0.2M NaCl and sonicated. After sonication, 3mg hexadecyltrimethylammonium bromide  
816 (CTAB) (Fisher Cat. No. 227160) per 1 mg precipitate was slowly added to the solution  
817 on low heat. After removing from heat, another 2.5 volumes of 0.5mg CTAB was added.  
818 The solution was centrifuged at 11,000xg for 2 hours, and the pellet washed in 10%  
819 EtOH to remove any remaining CTAB. After an additional centrifugation at 18,000xg,  
820 the pellet was resuspended in 1M NaCl and sonicated for 2 hours. Once the GXM was  
821 solubilized, it was dialyzed (3.5kDa cutoff) versus sterile distilled water and then  
822 lyophilized. Purified, lyophilized GXM was stored at -80°C for subsequent use.

823

824 Adherence assay: We used a slightly modified protocol of biofilm formation and 2,3-Bis-  
825 (2-Methoxy-4-Nitro-5-Sulfophenyl)-2H-Tetrazolium-5-Carboxanilide (XTT) analysis, as  
826 described previously (46, 47). Briefly, 5 mL cultures were grown overnight in  
827 YNB+2%glucose at 30 °C, pelleted, washed in 1X PBS, and resuspended in 1X PBS.

828 Cells were counted on a hemocytometer, diluted to  $10^7$  cells/mL in the appropriate  
829 media and plated in 100  $\mu$ l volumes in 96  $\mu$ l polystyrene plates (avoiding edge wells).  
830 Sterile media was plated as a negative control. Plates were incubated for 48 hours at  
831 37 °C to allow for adherence and biofilm maturation. Plates were then washed 3 times  
832 with 200  $\mu$ l of 1X PBS+0.05% tween-20 using a BioTek 405 TS microplate washer set  
833 to an intermediate flow rate. To determine the relative levels of cells that remained after  
834 washing, we used the XTT reduction assay to quantitate metabolic activity as a proxy  
835 for viable cell density. After plate washing, 100  $\mu$ l of a solution containing 0.5g/L XTT  
836 (Fisher Cat. No. X6493) and 4  $\mu$ M menadione (Sigma Cat. No. 58-27-5) in acetone in  
837 1X PBS was added to each well. Menadione was added to fresh XTT solution  
838 immediately prior to adding the solution to a plate. Plates were incubated for 5 hours  
839 before moving 80  $\mu$ l supernatant aliquots to a new plate to read absorbance at 490nm.  
840  
841 Mice: For the intranasal infection model, we used ~8-week-old female C57BL/6NJ mice  
842 (Jackson Labs). *C. neoformans* cells were harvested from overnight 30°C YPD cultures,  
843 washed two times in 1X PBS, resuspended in 1X PBS, and then counted with a  
844 hemocytometer to determine the inoculum. Mice were anesthetized with  
845 ketamine/dexdomitor (mg/g) intraperitoneally before suspending them on horizontally  
846 tied thread by their front incisors. Mice were kept warm with a heat lamp and inoculated  
847 intranasally with  $2.5 \times 10^4$  *C. neoformans* cells in 50  $\mu$ l 1X PBS. After 10 minutes, mice  
848 were removed from thread and administered the reversal agent antisedan  
849 (~0.0125mg/g) intraperitoneally. For survival analyses, mice were weighed daily and  
850 euthanized by CO<sub>2</sub> asphyxiation and cervical dislocation, when they lost 15% of their

851 initial mass. Mice used to analyze fungal burden, capsule size, and GXM levels were  
852 euthanized by the same measures at designated time points. Mice used for flow  
853 cytometry analysis were anesthetized with isoflurane and intracardially perfused with  
854 cold 1X PBS before cervical dislocation and brain extraction.

855 For the intracranial infection model, we used ~6-week-old female C57BL/6NJ  
856 mice (Jackson labs). *C. neoformans* inoculum was prepared as described above. Prior  
857 to inoculation, mice were anesthetized with ketamine/dexdomitor, as above. Mice were  
858 inoculated intracranially with 200 *C. neoformans* cells in 30 $\mu$ l 1X PBS via a 26Gx1/2  
859 needle. Animals were then administered antisedan to speed recovery.

860

861 Fungal Burden: Organs were harvested from euthanized mice, placed on ice, and  
862 homogenized with a Tissue Master Homogenizer (Omni International) in 5 mL 1X PBS.  
863 Serial dilutions of organ homogenates were plated on Sabouraud's dextrose agar with  
864 10mg/mL gentamycin and 100 mg/mL carbenicillin, and stored at 30°C in the dark for  
865 three days. Resulting colony forming units (CFU) were then counted to determine fungal  
866 burden.

867

868 GXM ELISA: 500  $\mu$ l of the same mouse organ homogenate used for CFU counts and *C.*  
869 *neoformans* cell measurements was collected and spun down at 3,000g for 5 minutes.  
870 The supernatant was then passed through a 0.22  $\mu$ m filter to remove cells. GXM levels  
871 in the resulting were quantified using the ALPHA Cryptococcal Antigen enzyme  
872 immunoassay (IMMY Ref. CRY101). GXM purified from *C. neoformans* cultures was  
873 diluted to generate standard curves.

874

875 Histology: Perfused mouse brains were divided in half and fixed overnight in 4%  
876 paraformaldehyde. 8 µm thick sagittal slices were mounted on microscope slides and  
877 stored at -20 °C. Successive sections were stained with hematoxylin and eosin or  
878 Grocott's methenamine silver (ThermoFisher Scientific Cat. No. 87008).

879

880 Flow cytometry: Perfused mouse brains were collected in RPMI, ground gently to  
881 disperse tissue and spun in a 90% Percoll (Sigma Cat. No. P1644) with a 63% Percoll  
882 underlay to isolate leukocytes at the interface. Leukocytes were resuspended in FACS  
883 buffer (1X PBS, 1% bovine serum albumin), and stained with the appropriate  
884 fluorescently labeled antibodies. Labeled cells were fixed for 20 minutes in 4%  
885 paraformaldehyde before analysis on a LSRFortessa (BD Biosciences). Antibodies  
886 used in this study (eBiosciences): CD45-eFluor450 (48-0451-82), CD4-APC (Cat. No.  
887 17-0041-82), CD8-FITC (11-0081-82), F4/80-FITC (11-4801-82), Ly6G-FITC (11-5931-  
888 82), Ly6C-APC (17-5932-82).

889

890 **References:**

891

- 892 1. May RC, Stone NRH, Wiesner DL, Bicanic T, Nielsen K. 2016. Cryptococcus:  
893 from environmental saprophyte to global pathogen. *Nat Rev Micro* 14:106-117.
- 894 2. Rajasingham R, Smith RM, Park BJ, Jarvis JN, Govender NP, Chiller TM,  
895 Denning DW, Loyse A, Boulware DR. 2017. Global burden of disease of HIV-  
896 associated cryptococcal meningitis: an updated analysis. *The Lancet Infectious  
897 Diseases* 17:873-881.
- 898 3. Goldman DL, Khine H, Abadi J, Lindenberg DJ, Pirofski L-a, Niang R, Casadevall  
899 A. 2001. Serologic Evidence for *Cryptococcus neoformans* Infection in Early  
900 Childhood. *Pediatrics* 107:e66-e66.
- 901 4. Garcia-Hermoso D, Janbon G, Dromer F. 1999. Epidemiological Evidence for  
902 Dormant *Cryptococcus neoformans* Infection. *Journal of Clinical Microbiology*  
903 37:3204-3209.

904 5. Idnurm A, Bahn Y-S, Nielsen K, Lin X, Fraser JA, Heitman J. 2005. Deciphering  
905 the Model Pathogenic Fungus *Cryptococcus Neoformans*. *Nat Rev Micro* 3:753-  
906 764.

907 6. Chen Y, Toffaletti DL, Tenor JL, Litvintseva AP, Fang C, Mitchell TG, McDonald  
908 TR, Nielsen K, Boulware DR, Bicanic T, Perfect JR. 2014. The *Cryptococcus*  
909 *neoformans* Transcriptome at the Site of Human Meningitis. *mBio* 5:e01087-13.

910 7. van de Beek D, de Gans J, Tunkel AR, Wijdicks EFM. 2006. Community-  
911 Acquired Bacterial Meningitis in Adults. *New England Journal of Medicine*  
912 354:44-53.

913 8. Kim JV, Kang SS, Dustin ML, McGavern DB. 2009. Myelomonocytic cell  
914 recruitment causes fatal CNS vascular injury during acute viral meningitis. *Nature*  
915 457:191-195.

916 9. Chuck SL, Sande MA. 1989. Infections with *Cryptococcus neoformans* in the  
917 Acquired Immunodeficiency Syndrome. *New England Journal of Medicine*  
918 321:794-799.

919 10. Robertson EJ, Najjuka G, Rolfes MA, Akampurira A, Jain N, Anantharanjit J, von  
920 Hohenberg M, Tassieri M, Carlsson A, Meya DB, Harrison TS, Fries BC,  
921 Boulware DR, Bicanic T. 2014. *Cryptococcus neoformans* Ex Vivo Capsule Size  
922 Is Associated With Intracranial Pressure and Host Immune Response in HIV-  
923 associated Cryptococcal Meningitis. *The Journal of Infectious Diseases* 209:74-  
924 82.

925 11. Olszewski MA, Noverr MC, Chen G-H, Toews GB, Cox GM, Perfect JR,  
926 Huffnagle GB. 2004. Urease Expression by *Cryptococcus neoformans* Promotes  
927 Microvascular Sequestration, Thereby Enhancing Central Nervous System  
928 Invasion. *The American Journal of Pathology* 164:1761-1771.

929 12. Jarvis JN, Meintjes G, Bicanic T, Buffa V, Hogan L, Mo S, Tomlinson G, Kropf P,  
930 Noursadeghi M, Harrison TS. 2015. Cerebrospinal Fluid Cytokine Profiles Predict  
931 Risk of Early Mortality and Immune Reconstitution Inflammatory Syndrome in  
932 HIV-Associated Cryptococcal Meningitis. *PLoS Pathogens* 11:e1004754.

933 13. Boulware DR, Bonham SC, Meya DB, Wiesner DL, Park GS, Kambugu A, Janoff  
934 EN, Bohjanen PR. 2010. Paucity of Initial Cerebrospinal Fluid Inflammation in  
935 Cryptococcal Meningitis is associated with subsequent Immune Reconstitution  
936 Inflammatory Syndrome. *The Journal of infectious diseases* 202:962-970.

937 14. Zaragoza O, Nielsen K. 2013. Titan cells in *Cryptococcus neoformans*: Cells with  
938 a giant impact. *Current opinion in microbiology* 16:409-413.

939 15. O'Meara TR, Alspaugh JA. 2012. The *Cryptococcus neoformans* Capsule: a  
940 Sword and a Shield. *Clinical Microbiology Reviews* 25:387-408.

941 16. Doering TL. 2009. How Sweet it is! Cell Wall Biogenesis and Polysaccharide  
942 Capsule Formation in *Cryptococcus neoformans*. *Annual review of microbiology*  
943 63:223-247.

944 17. Zaragoza O, Taborda CP, Casadevall A. 2003. The efficacy of complement-  
945 mediated phagocytosis of *Cryptococcus neoformans* is dependent on the  
946 location of C3 in the polysaccharide capsule and involves both direct and  
947 indirect C3-mediated interactions. *European Journal of Immunology* 33:1957-  
948 1967.

949 18. Zaragoza O, Chrisman CJ, Castelli MV, Frases S, Cuenca-Estrella M,  
950 Rodríguez-Tudela JL, Casadevall A. 2008. Capsule enlargement in  
951 *Cryptococcus neoformans* confers resistance to oxidative stress suggesting a  
952 mechanism for intracellular survival. *Cellular microbiology* 10:2043-2057.

953 19. Vecchiarelli A, Pericolini E, Gabrielli E, Kenno S, Perito S, Cenci E, Monari C.  
954 2013. Elucidating the immunological function of the *Cryptococcus neoformans*  
955 capsule. *Future Microbiology* 8:1107-1116.

956 20. Vecchiarelli A, Retini C, Monari C, Tascini C, Bistoni F, Kozel TR. 1996. Purified  
957 capsular polysaccharide of *Cryptococcus neoformans* induces interleukin-10  
958 secretion by human monocytes. *Infection and Immunity* 64:2846-2849.

959 21. Monari C, Bistoni F, Casadevall A, Pericolini E, Pietrella D, Kozel TR,  
960 Vecchiarelli A. 2005. Glucuronoxylomannan, a Microbial Compound, Regulates  
961 Expression of Costimulatory Molecules and Production of Cytokines in  
962 Macrophages. *The Journal of Infectious Diseases* 191:127-137.

963 22. Retini C, Kozel TR, Pietrella D, Monari C, Bistoni F, Vecchiarelli A. 2001.  
964 Interdependency of Interleukin-10 and Interleukin-12 in Regulation of T-Cell  
965 Differentiation and Effector Function of Monocytes in Response to Stimulation  
966 with *Cryptococcus neoformans*. *Infection and Immunity* 69:6064-6073.

967 23. Vecchiarelli A, Retini C, Pietrella D, Monari C, Tascini C, Beccari T, Kozel TR.  
968 1995. Downregulation by cryptococcal polysaccharide of tumor necrosis factor  
969 alpha and interleukin-1 beta secretion from human monocytes. *Infection and*  
970 *Immunity* 63:2919-2923.

971 24. Retini C, Vecchiarelli A, Monari C, Bistoni F, Kozel TR. 1998. Encapsulation of  
972 *Cryptococcus neoformans* with Glucuronoxylomannan Inhibits the Antigen-  
973 Presenting Capacity of Monocytes. *Infection and Immunity* 66:664-669.

974 25. Vecchiarelli A, Pietrella D, Lupo P, Bistoni F, McFadden DC, Casadevall A. 2003.  
975 The polysaccharide capsule of *Cryptococcus neoformans* interferes with human  
976 dendritic cell maturation and activation. *Journal of Leukocyte Biology* 74:370-378.

977 26. Villena SN, Pinheiro RO, Pinheiro CS, Nunes MP, Takiya CM, DosReis GA,  
978 Previato JO, Mendonça-Previato L, Freire-de-Lima CG. 2008. Capsular  
979 polysaccharides galactoxylomannan and glucuronoxylomannan from  
980 *Cryptococcus neoformans* induce macrophage apoptosis mediated by Fas  
981 ligand. *Cellular Microbiology* 10:1274-1285.

982 27. Ellerbroek PM, Hoepelman AIM, Wolbers F, Zwaginga JJ, Coenjaerts FEJ. 2002.  
983 Cryptococcal Glucuronoxylomannan Inhibits Adhesion of Neutrophils to  
984 Stimulated Endothelium In Vitro by Affecting Both Neutrophils and Endothelial  
985 Cells. *Infection and Immunity* 70:4762-4771.

986 28. Dong ZM, Murphy JW. 1995. Intravascular cryptococcal culture filtrate (CneF)  
987 and its major component, glucuronoxylomannan, are potent inhibitors of  
988 leukocyte accumulation. *Infection and Immunity* 63:770-778.

989 29. Dong ZM, Murphy JW. 1996. Cryptococcal polysaccharides induce L-selectin  
990 shedding and tumor necrosis factor receptor loss from the surface of human  
991 neutrophils. *Journal of Clinical Investigation* 97:689-698.

992 30. Cherniak R, Morris LC, Anderson BC, Meyer SA. 1991. Facilitated isolation,  
993 purification, and analysis of glucuronoxylomannan of *Cryptococcus neoformans*.  
994 *Infection and Immunity* 59:59-64.

995 31. Jarvis JN, Percival A, Bauman S, Pelfrey J, Meintjes G, Williams GN, Longley N,  
996 Harrison TS, Kozel TR. 2011. Evaluation of a Novel Point-of-Care Cryptococcal  
997 Antigen Test on Serum, Plasma, and Urine From Patients With HIV-Associated  
998 Cryptococcal Meningitis. *Clinical Infectious Diseases: An Official Publication of  
999 the Infectious Diseases Society of America* 53:1019-1023.

1000 32. Scriven JE, Graham LM, Schutz C, Scriba TJ, Wilkinson KA, Wilkinson RJ,  
1001 Boulware DR, Urban BC, Laloo DG, Meintjes G. 2016. A Glucuronoxylomannan-  
1002 Associated Immune Signature, Characterized by Monocyte Deactivation and an  
1003 Increased Interleukin 10 Level, Is a Predictor of Death in Cryptococcal  
1004 Meningitis. *The Journal of Infectious Diseases* 213:1725-1734.

1005 33. Buchanan KL, Murphy JW. 1998. What makes *Cryptococcus neoformans* a  
1006 pathogen? *Emerging Infectious Diseases* 4:71-83.

1007 34. Frases S, Nimrichter L, Viana NB, Nakouzi A, Casadevall A. 2008. *Cryptococcus  
1008 neoformans* Capsular Polysaccharide and Exopolysaccharide Fractions Manifest  
1009 Physical, Chemical, and Antigenic Differences. *Eukaryotic Cell* 7:319-327.

1010 35. Yoneda A, Doering TL. 2008. Regulation of *Cryptococcus neoformans* Capsule  
1011 Size Is Mediated at the Polymer Level. *Eukaryotic Cell* 7:546-549.

1012 36. Cordero RJB, Frases S, Guimarães AJ, Rivera J, Casadevall A. 2011. Evidence  
1013 for Branching in Cryptococcal Capsular Polysaccharides and Consequences on  
1014 its Biological Activity. *Molecular microbiology* 79:1101-1117.

1015 37. de S. Araújo GR, Fontes GN, Leão D, Rocha GM, Pontes B, Sant'Anna C, de  
1016 Souza W, Frases S. 2016. *Cryptococcus neoformans* capsular polysaccharides  
1017 form branched and complex filamentous networks viewed by high-resolution  
1018 microscopy. *Journal of Structural Biology* 193:75-82.

1019 38. Kozel TR, Levitz SM, Dromer F, Gates MA, Thorkildson P, Janbon G. 2003.  
1020 Antigenic and Biological Characteristics of Mutant Strains of *Cryptococcus  
1021 neoformans* Lacking Capsular O Acetylation or Xylosyl Side Chains. *Infection  
1022 and Immunity* 71:2868-2875.

1023 39. Urai M, Kaneko Y, Ueno K, Okubo Y, Aizawa T, Fukazawa H, Sugita T, Ohno H,  
1024 Shibuya K, Kinjo Y, Miyazaki Y. 2015. Evasion of Innate Immune Responses by  
1025 the Highly Virulent *Cryptococcus gattii* by Altering Capsule  
1026 Glucuronoxylomannan Structure. *Frontiers in Cellular and Infection Microbiology*  
1027 5:101.

1028 40. Ellerbroek PM, Lefeber DJ, van Veghel R, Scharringa J, Brouwer E, Gerwig GJ,  
1029 Janbon G, Hoepelman AIM, Coenjaerts FEJ. 2004. O-Acetylation of  
1030 Cryptococcal Capsular Glucuronoxylomannan Is Essential for Interference with  
1031 Neutrophil Migration. *The Journal of Immunology* 173:7513.

1032 41. Janbon G, Himmelreich U, Moyrand F, Improvisi L, Dromer F. 2001. Cas1p is a  
1033 membrane protein necessary for the O-acetylation of the *Cryptococcus  
1034 neoformans* capsular polysaccharide. *Molecular Microbiology* 42:453-467.

1035 42. Liu OW, Chun CD, Chow ED, Chen C, Madhani HD, Noble SM. 2008.  
1036 Systematic genetic analysis of virulence in the human fungal pathogen  
1037 *Cryptococcus neoformans*. *Cell* 135:174-188.

1038 43. Willment JA, Brown GD. 2008. C-type lectin receptors in antifungal immunity.  
1039 Trends in Microbiology 16:27-32.

1040 44. Brown JCS, Madhani HD. 2012. Approaching the Functional Annotation of  
1041 Fungal Virulence Factors Using Cross-Species Genetic Interaction Profiling.  
1042 PLOS Genetics 8:e1003168.

1043 45. Martinez LR, Casadevall A. 2015. Biofilm Formation by *Cryptococcus*  
1044 *neoformans*. Microbiology Spectrum 3.

1045 46. Martinez LR, Casadevall A. 2005. Specific Antibody Can Prevent Fungal Biofilm  
1046 Formation and This Effect Correlates with Protective Efficacy. Infection and  
1047 Immunity 73:6350-6362.

1048 47. Pierce CG, Uppuluri P, Tristan AR, Wormley FL, Mowat E, Ramage G, Lopez-  
1049 Ribot JL. 2008. A simple and reproducible 96 well plate-based method for the  
1050 formation of fungal biofilms and its application to antifungal susceptibility testing.  
1051 Nature protocols 3:1494-1500.

1052 48. Vidal JE, Boulware DR. 2015. Lateral Flow Assay for Cryptococcal Antigen: an  
1053 Important Advance to Improve the Continuum of HIV Care and Reduce  
1054 Cryptococcal Meningitis-Related Mortality. Revista do Instituto de Medicina  
1055 Tropical de São Paulo 57:38-45.

1056 49. García-Barbazán I, Trevijano-Contador N, Rueda C, de Andrés B, Pérez-Tavárez  
1057 R, Herrero-Fernández I, Gaspar ML, Zaragoza O. 2016. The formation of titan  
1058 cells in *Cryptococcus neoformans* depends on the mouse strain and correlates  
1059 with induction of Th2-type responses. Cellular Microbiology 18:111-124.

1060 50. Okagaki LH, Strain AK, Nielsen JN, Charlier C, Baltes NJ, Chrétien F, Heitman J,  
1061 Dromer F, Nielsen K. 2010. Cryptococcal Cell Morphology Affects Host Cell  
1062 Interactions and Pathogenicity. PLoS Pathogens 6:e1000953.

1063 51. Zaragoza O, García-Rodas R, Nosanchuk JD, Cuenca-Estrella M, Rodríguez-  
1064 Tudela JL, Casadevall A. 2010. Fungal Cell Gigantism during Mammalian  
1065 Infection. PLoS Pathogens 6:e1000945.

1066 52. Maier EJ, Haynes BC, Gish SR, Wang ZA, Skowyra ML, Marulli AL, Doering TL,  
1067 Brent MR. 2015. Model-driven mapping of transcriptional networks reveals the  
1068 circuitry and dynamics of virulence regulation. Genome Research 25:690-700.

1069 53. Rizzo J, Oliveira DL, Joffe LS, Hu G, Gazos-Lopes F, Fonseca FL, Almeida IC,  
1070 Frases S, Kronstad JW, Rodrigues ML. 2014. Role of the Apt1 Protein in  
1071 Polysaccharide Secretion by *Cryptococcus neoformans*. Eukaryotic Cell 13:715-  
1072 726.

1073 54. Rivera J, Feldmesser M, Cammer M, Casadevall A. 1998. Organ-Dependent  
1074 Variation of Capsule Thickness in *Cryptococcus neoformans* during Experimental  
1075 Murine Infection. Infection and Immunity 66:5027-5030.

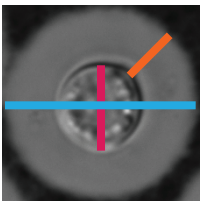
1076 55. Trevijano-Contador N, Rueda C, Zaragoza O. 2016. Fungal morphogenetic  
1077 changes inside the mammalian host. Seminars in Cell & Developmental Biology  
1078 57:100-109.

1079 56. Lipovsky MM, Tsenova L, Coenjaerts FEJ, Kaplan G, Cherniak R, Hoepelman  
1080 AIM. 2000. Cryptococcal glucuronoxylomannan delays translocation of  
1081 leukocytes across the blood–brain barrier in an animal model of acute bacterial  
1082 meningitis. Journal of Neuroimmunology 111:10-14.

1083  
1084

**Figure 1**

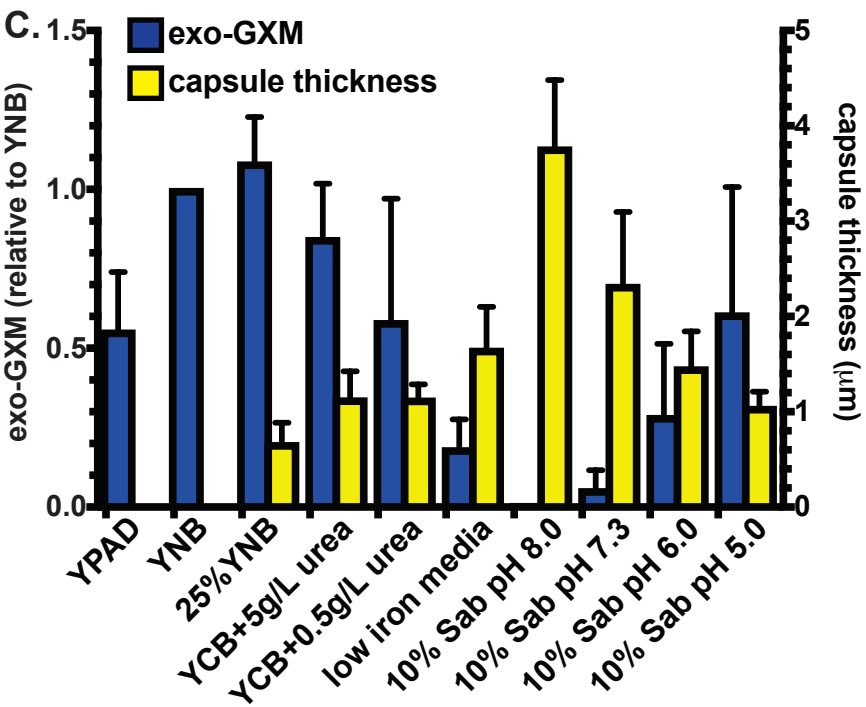
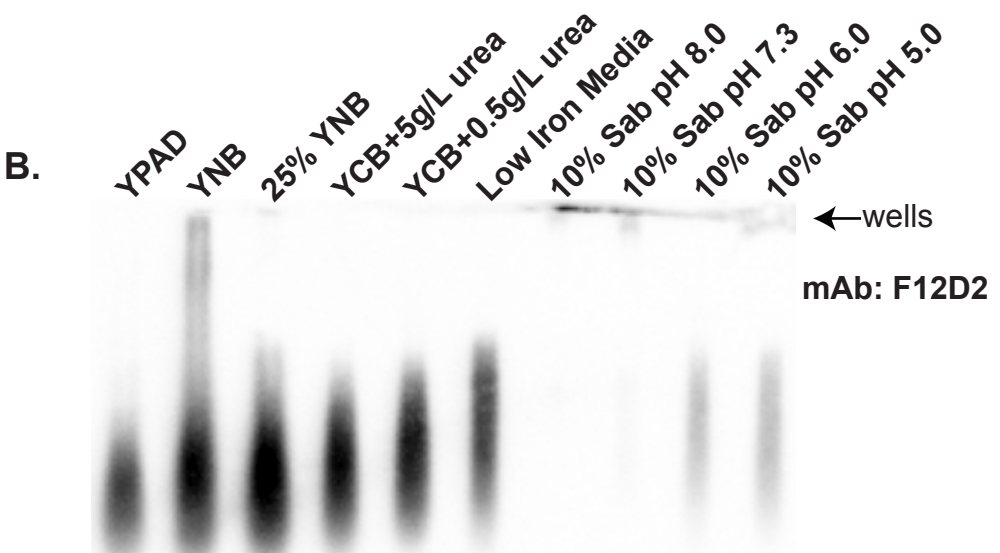
**A.**



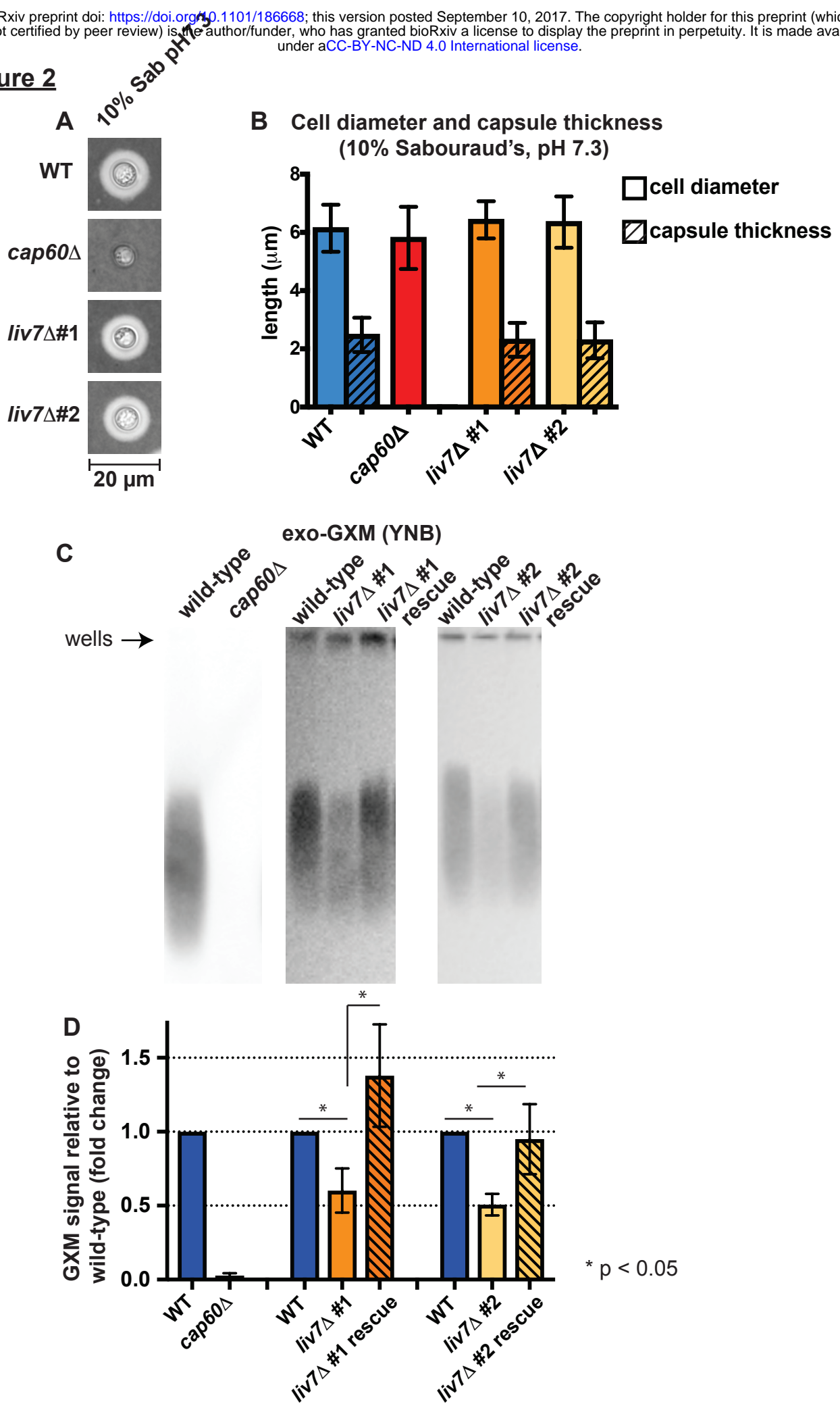
**total diameter**

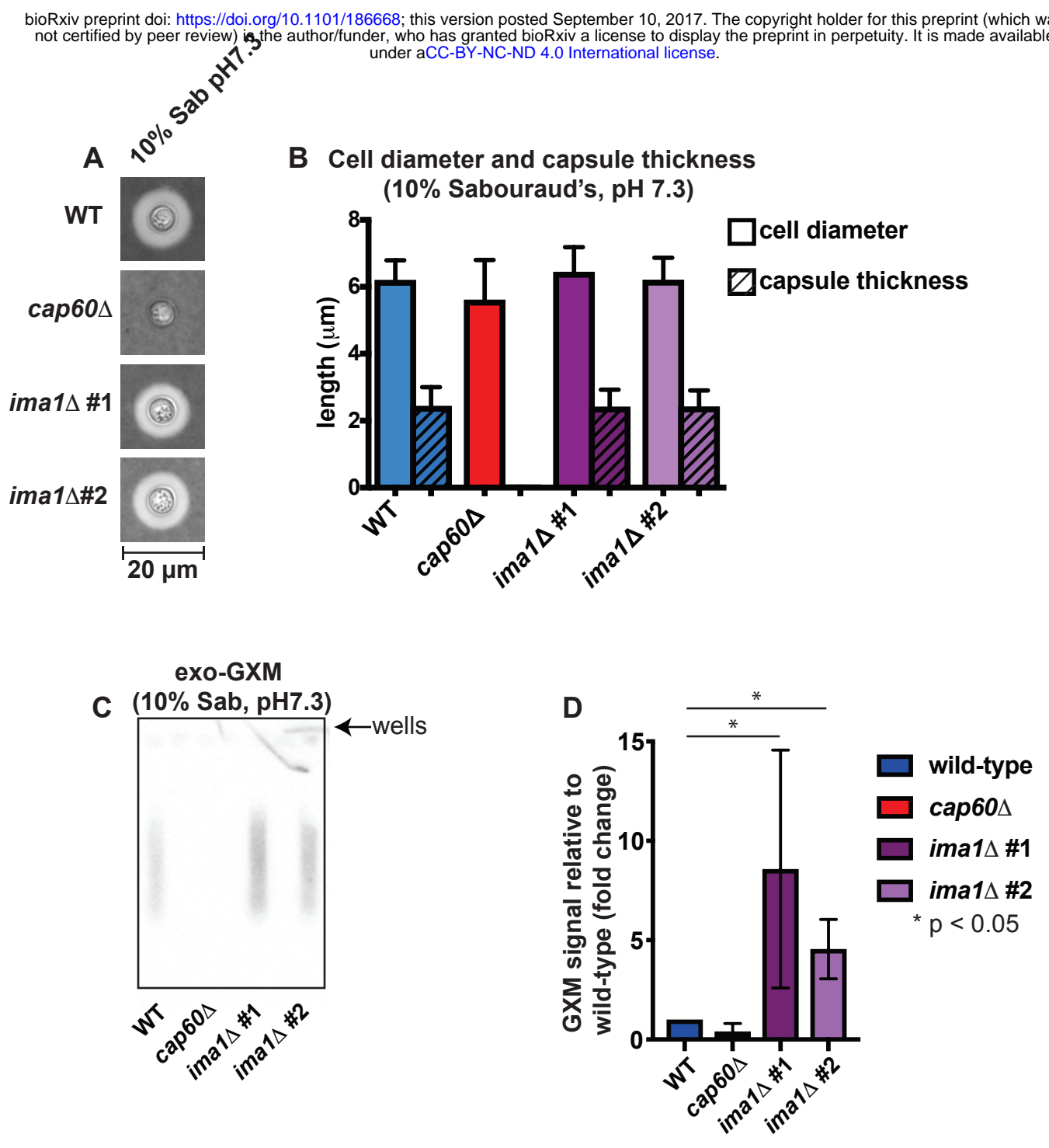
**cell body diameter**

**capsule thickness**



**Figure 2**





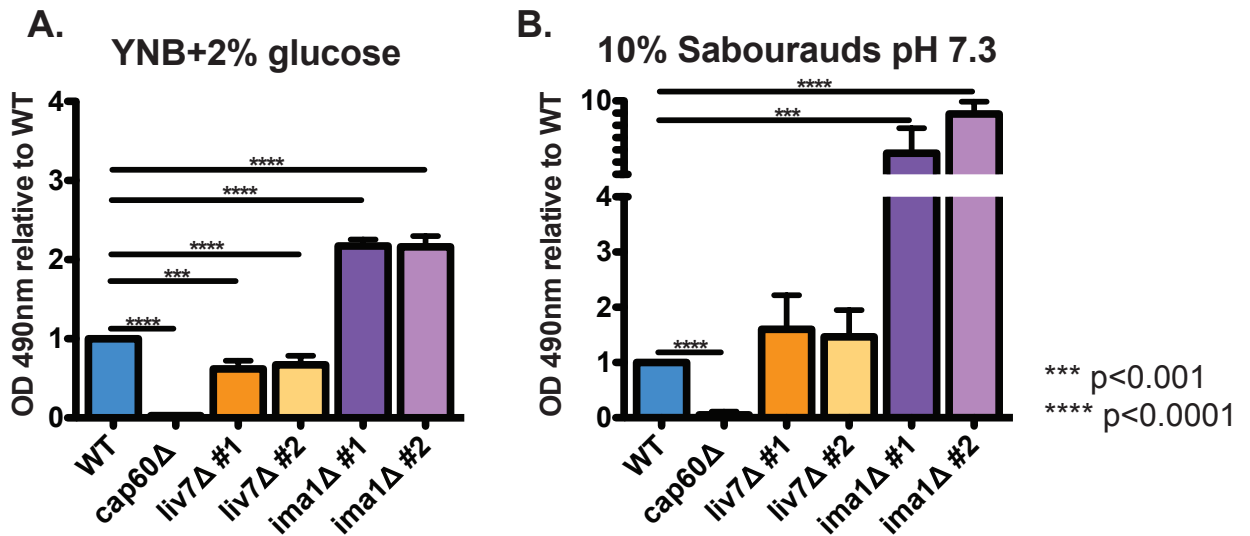


## Figure 5

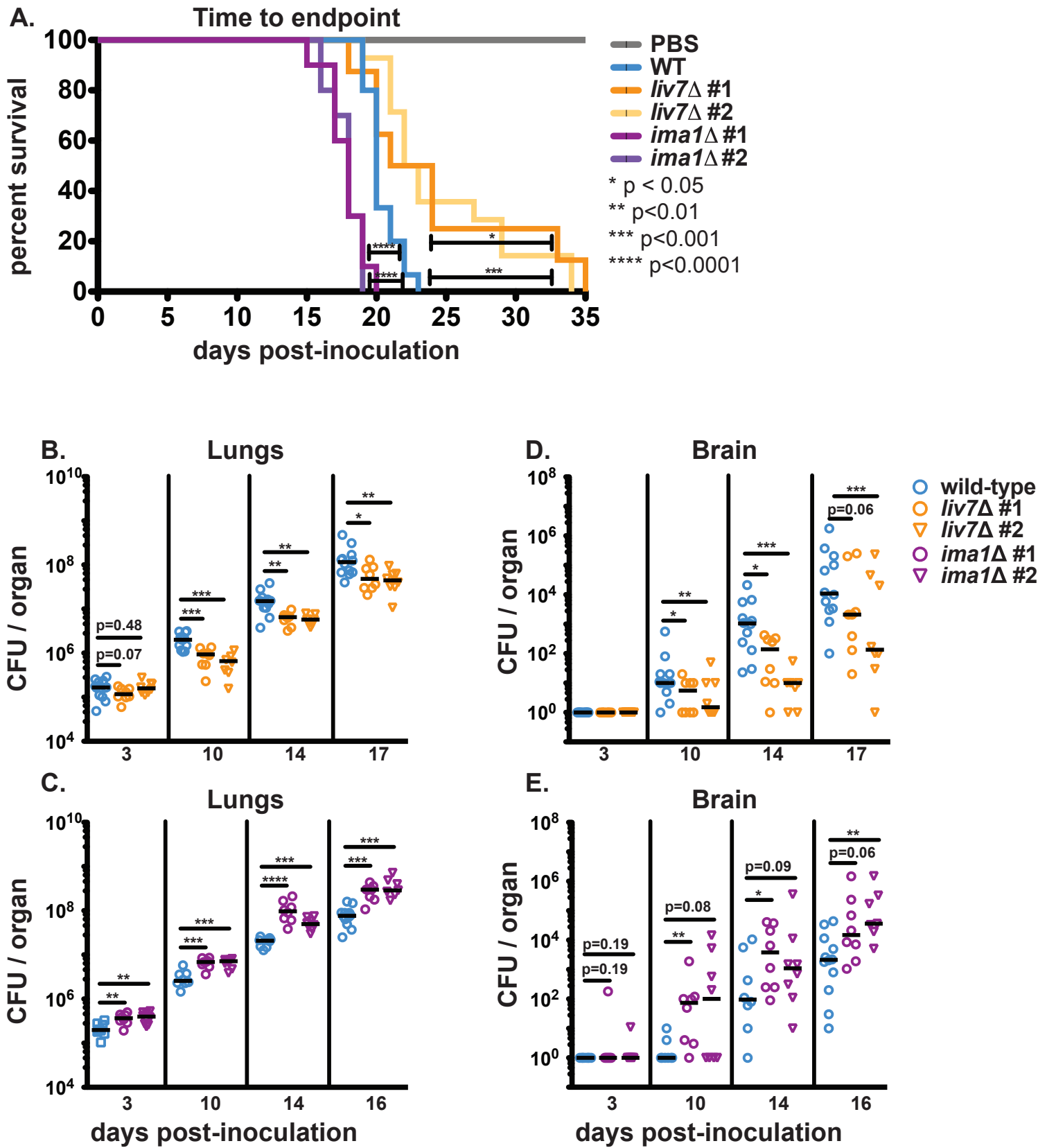
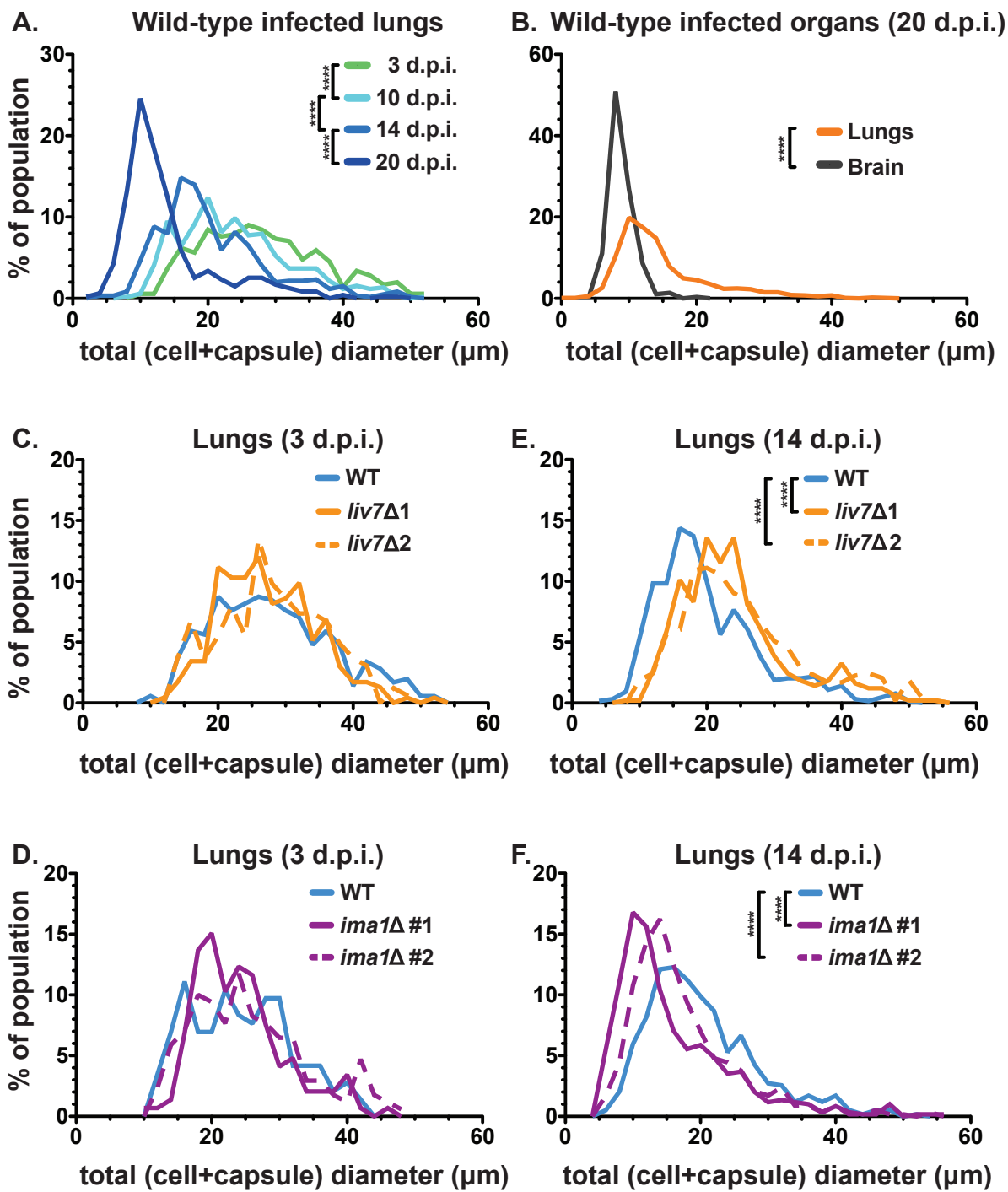


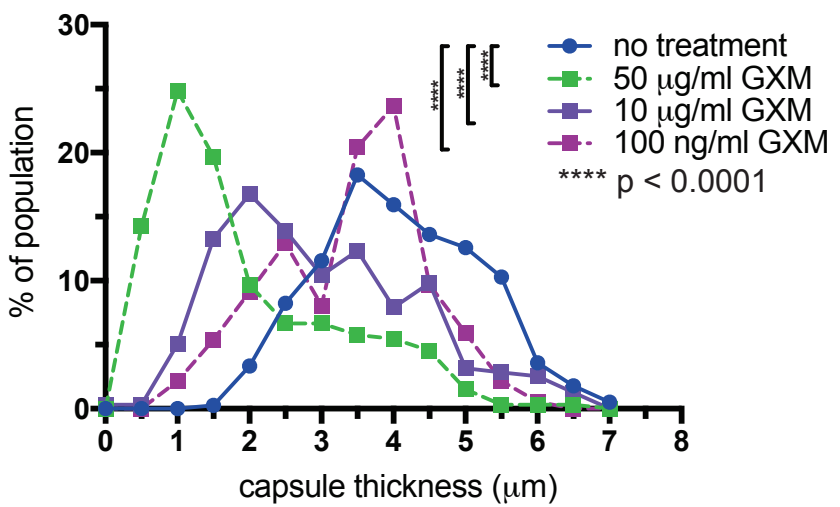
## Figure 6



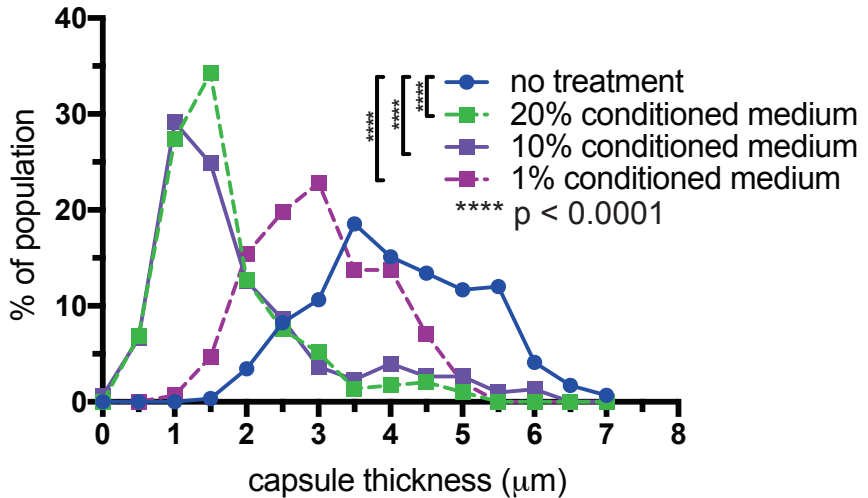
\*\*\*\*  $p < 0.0001$

## Figure 7

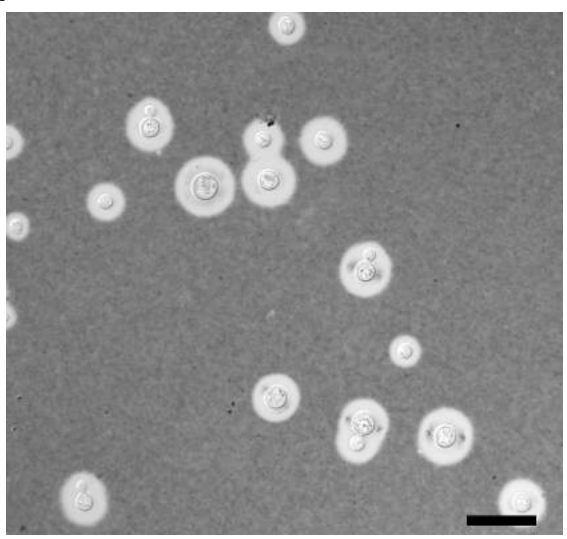
A.



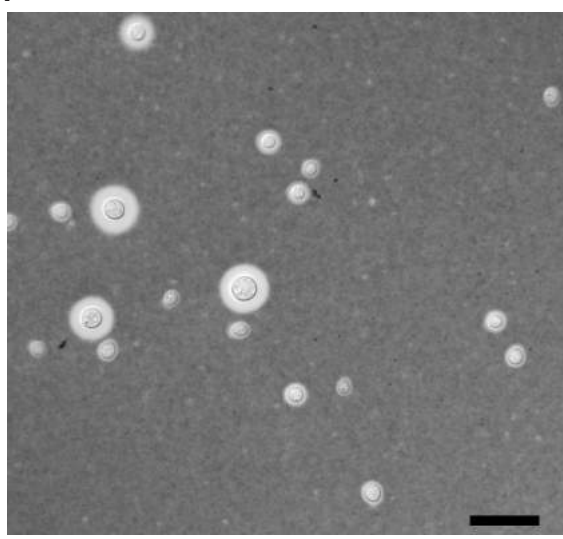
B.



C.



D.



scale=20µm

**Figure 8**

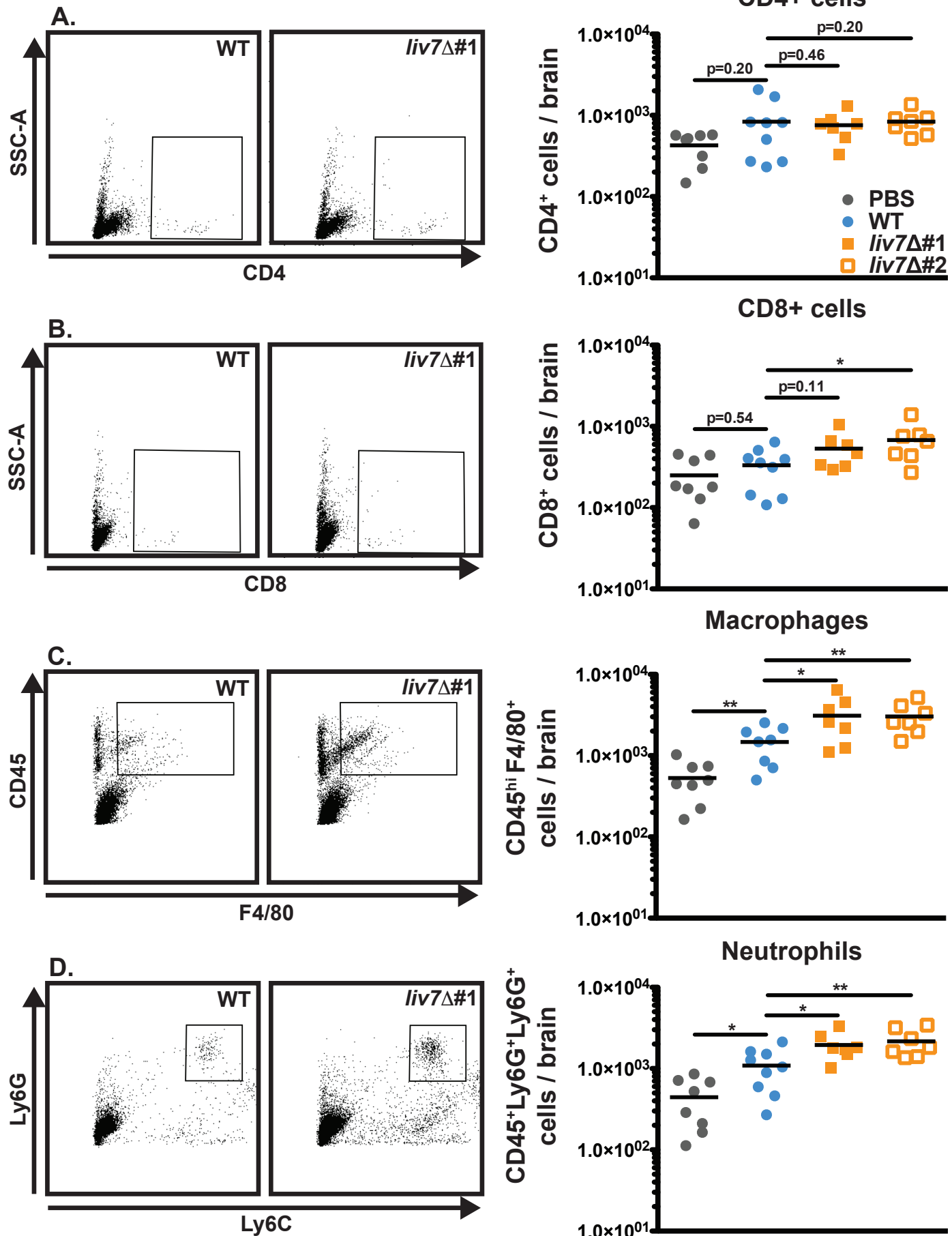


### Figure 9

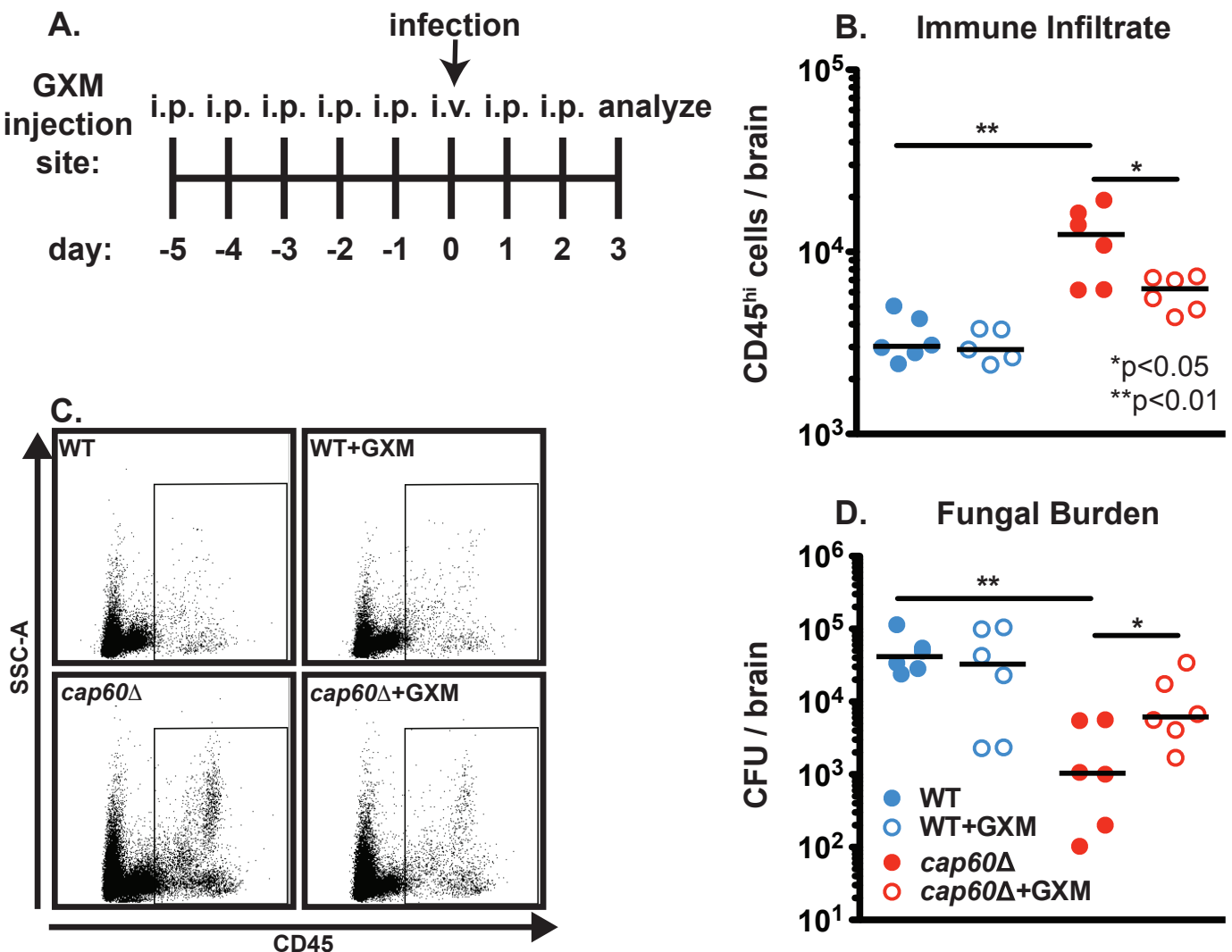
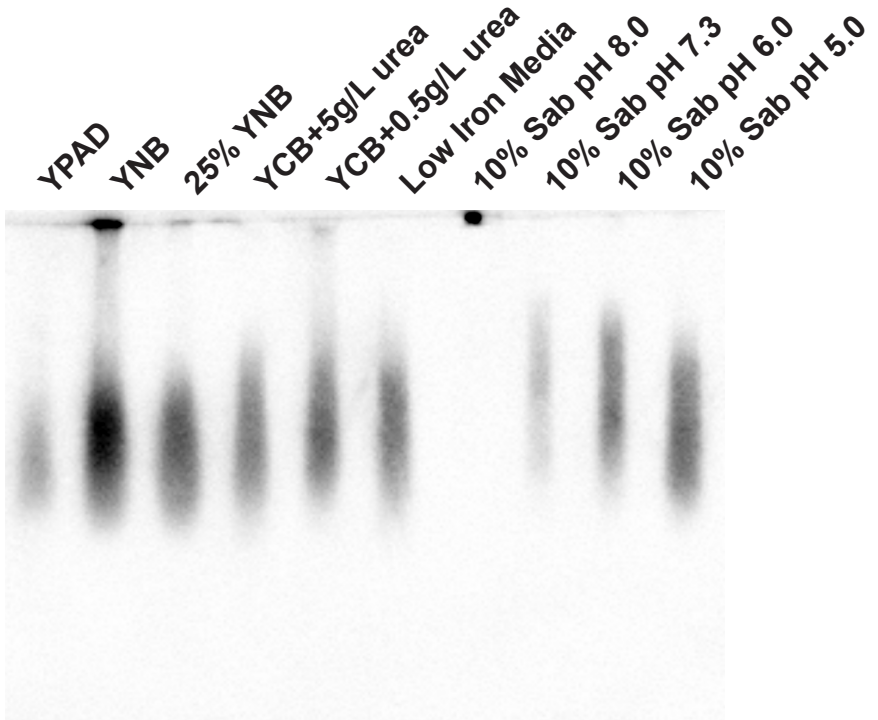


## **Figure S1**

### **A. F12D2**

**O-acetyl (+) GXM binding**  
**O-acetyl (-) GXM binding**



### **B. 1326**

**O-acetyl (+) GXM binding**

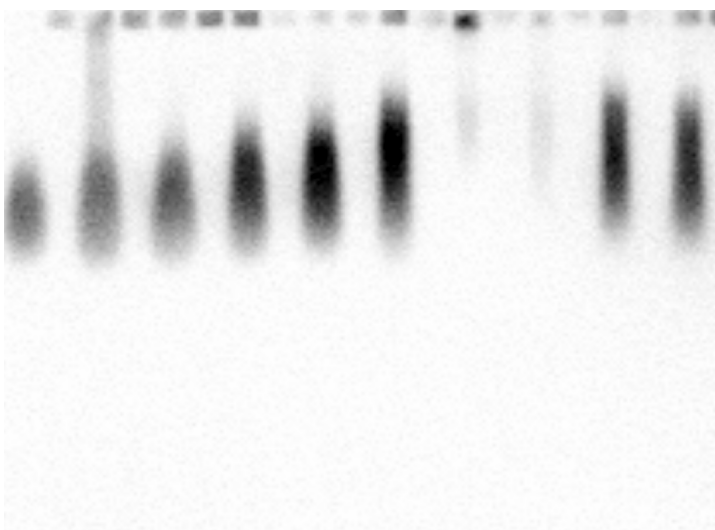


## Figure S2

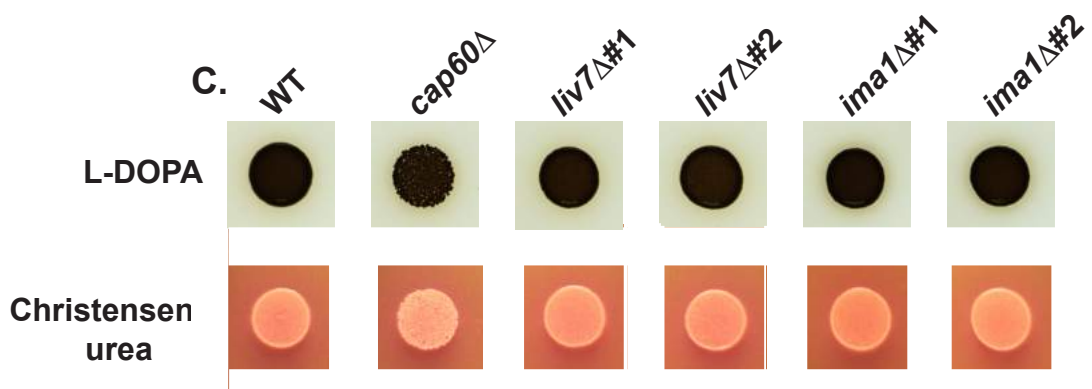
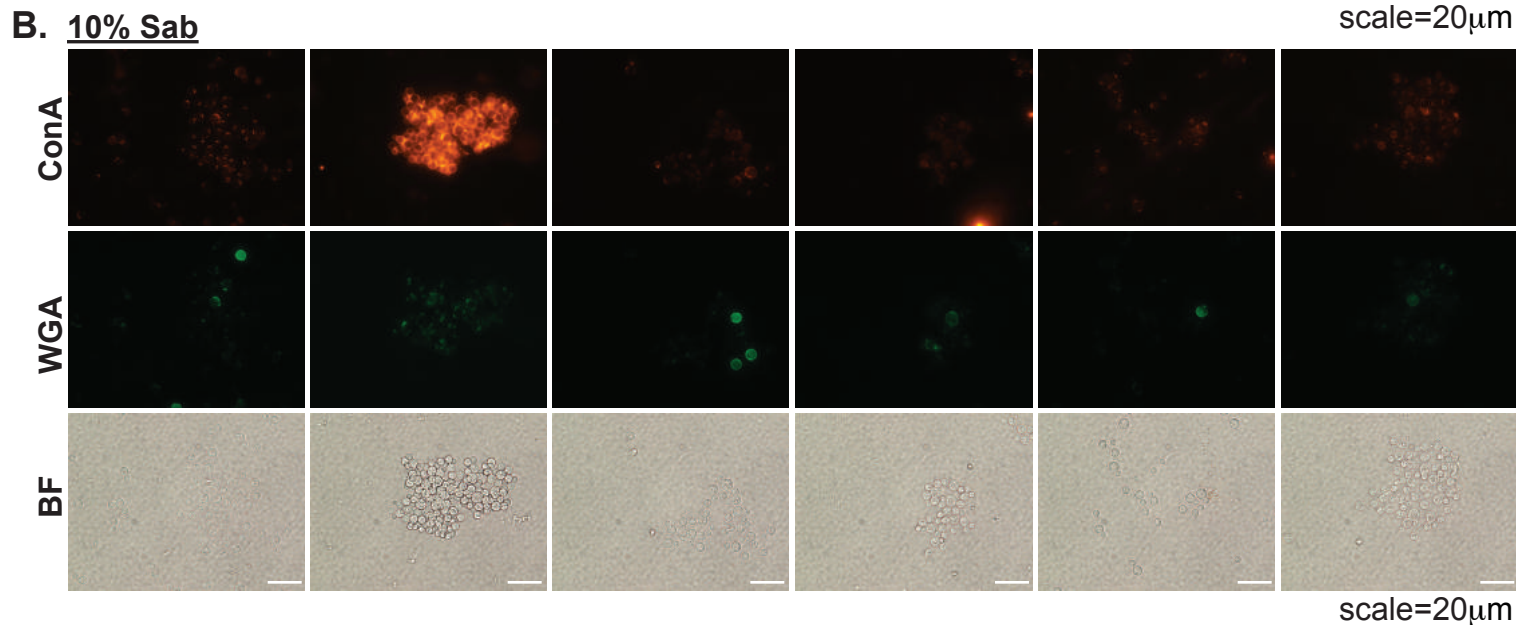
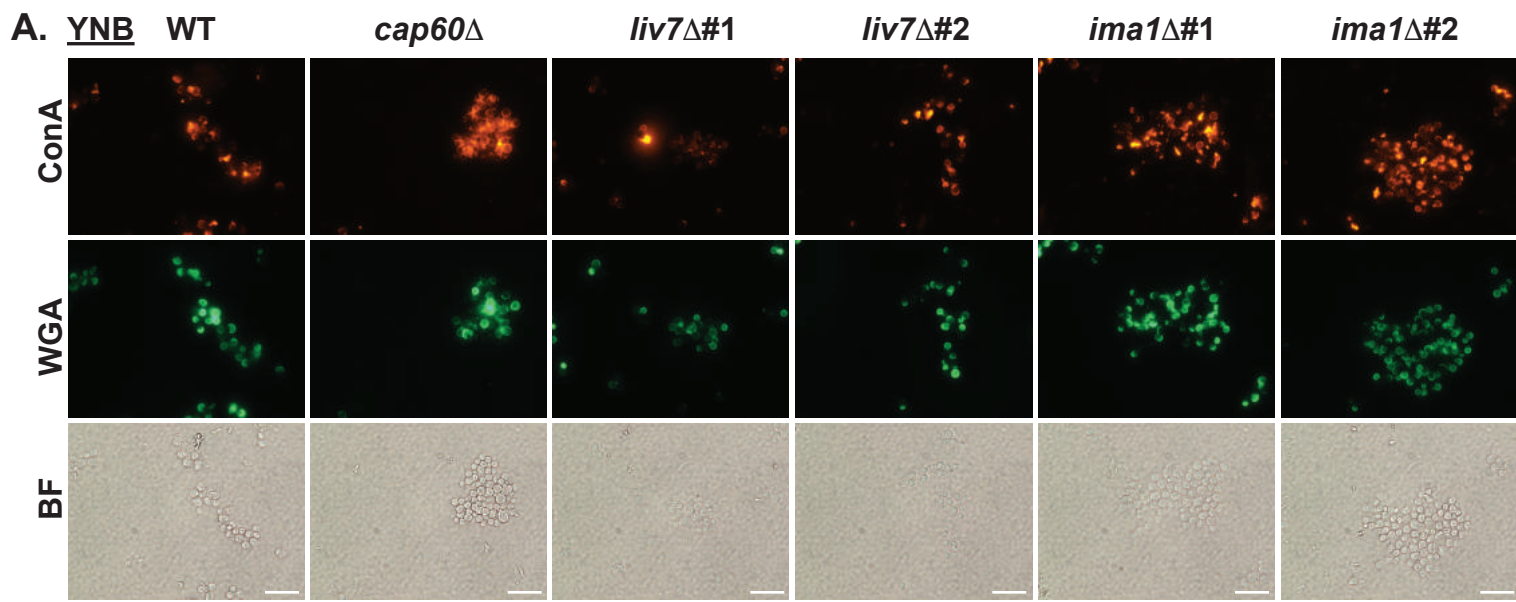


**Figure S3**

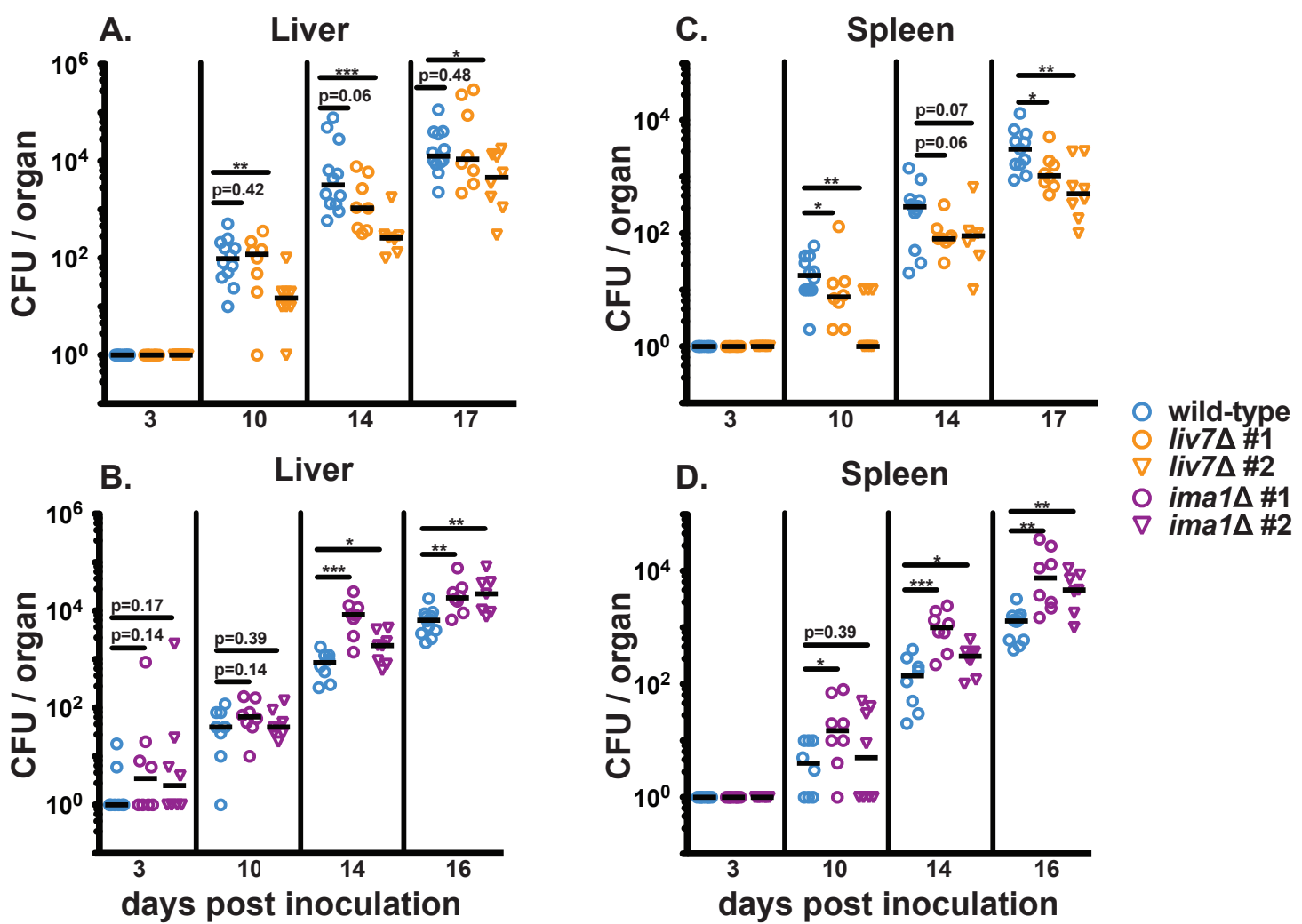
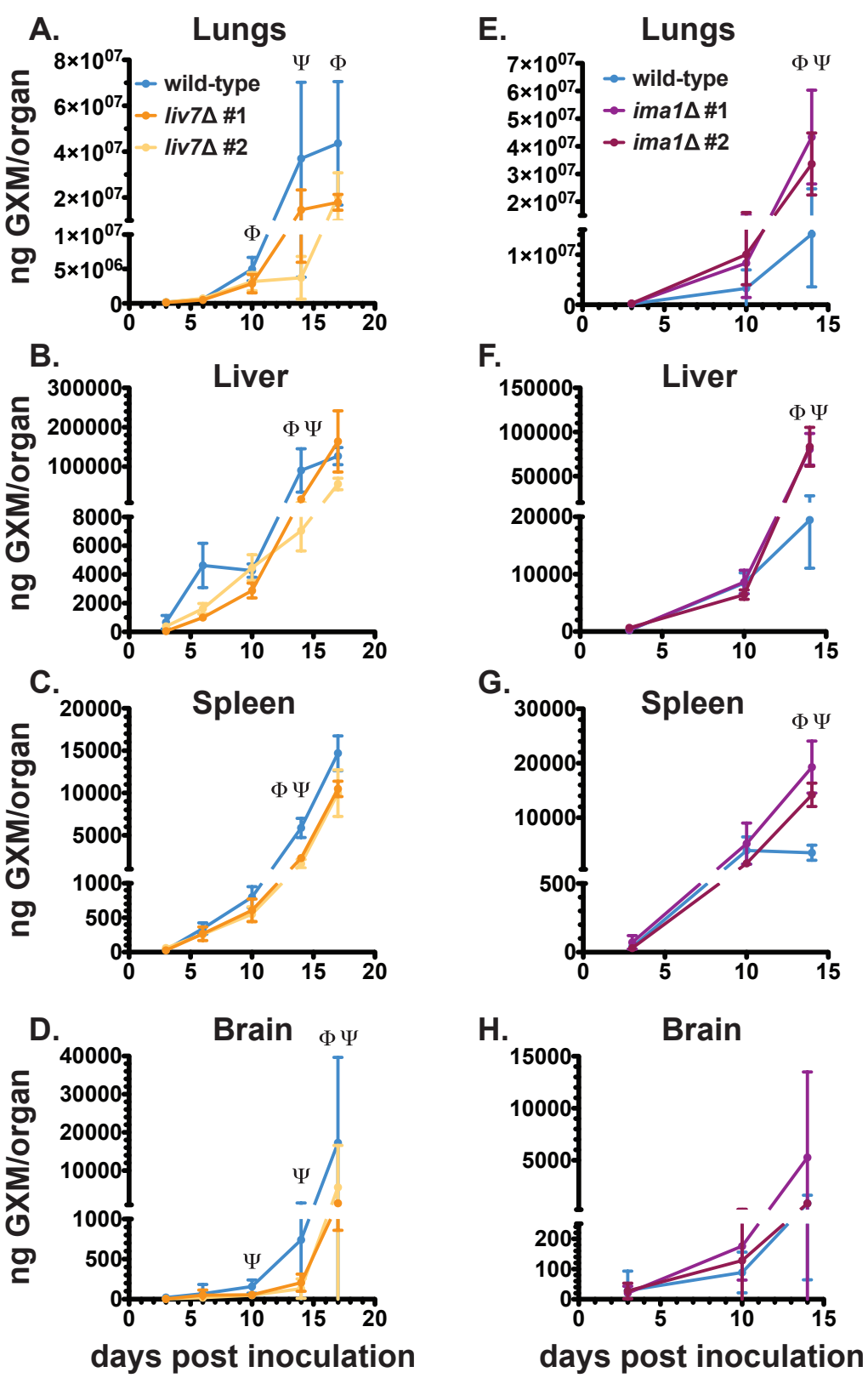


**Figure S4**

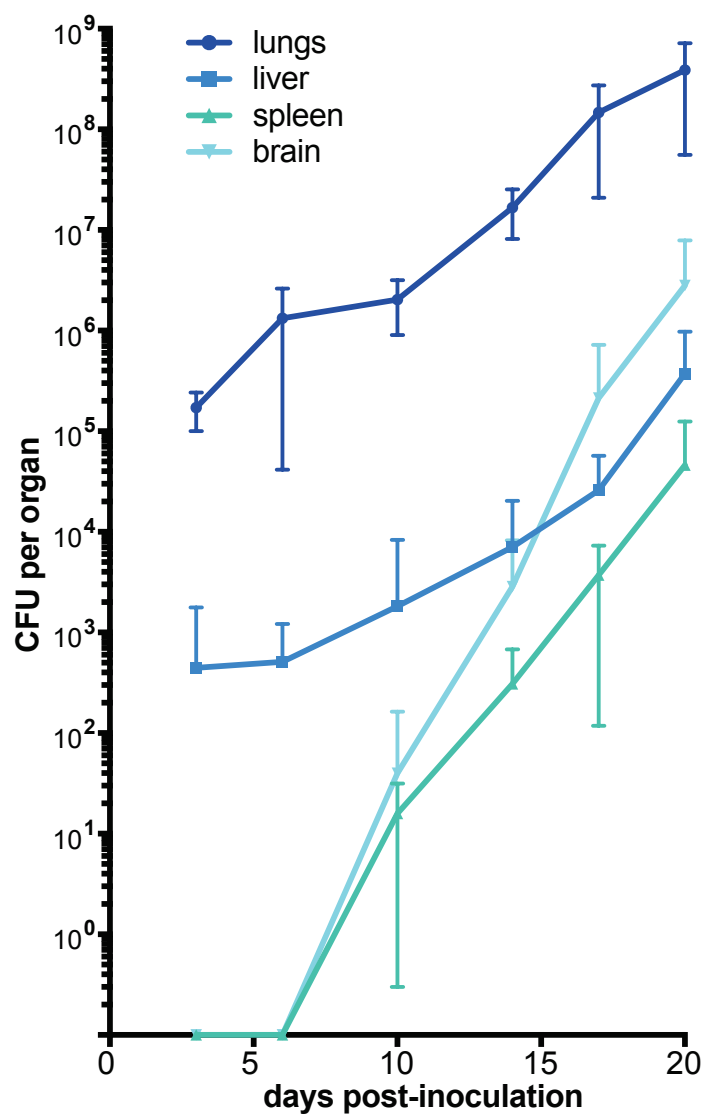


Φ  $p < 0.05$  (wild-type versus independent ko #1)

Ψ  $p < 0.05$  (wild-type versus independent ko #2)

## Figure S5

A.



B.

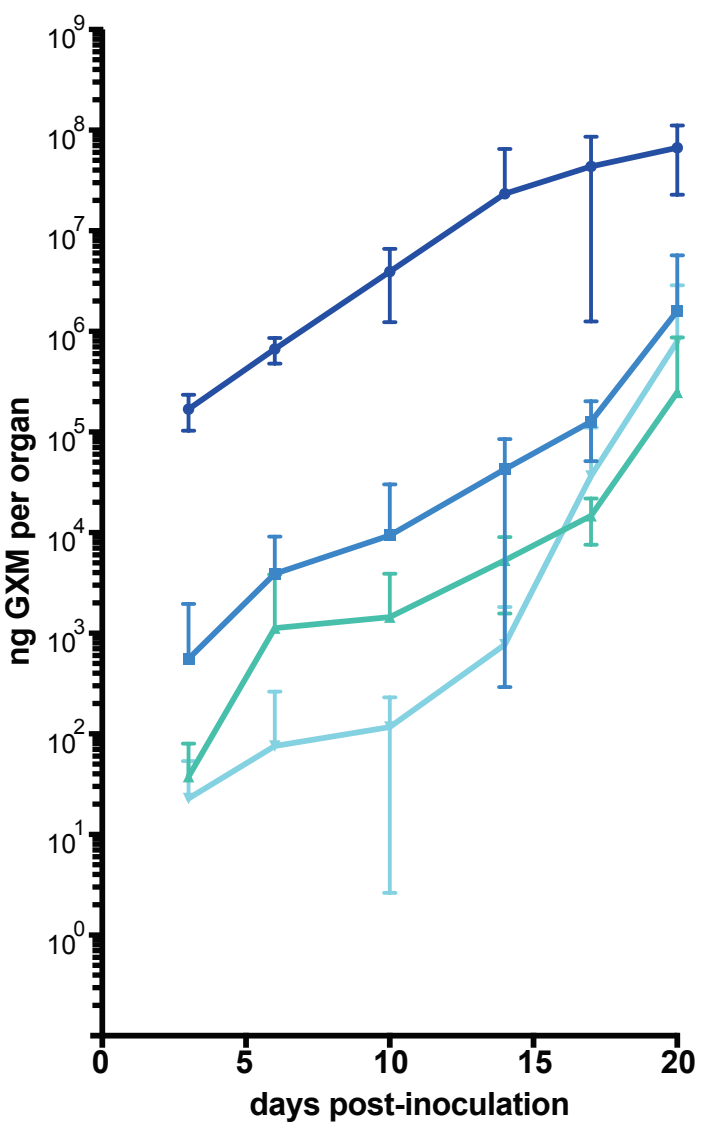


## Figure S6

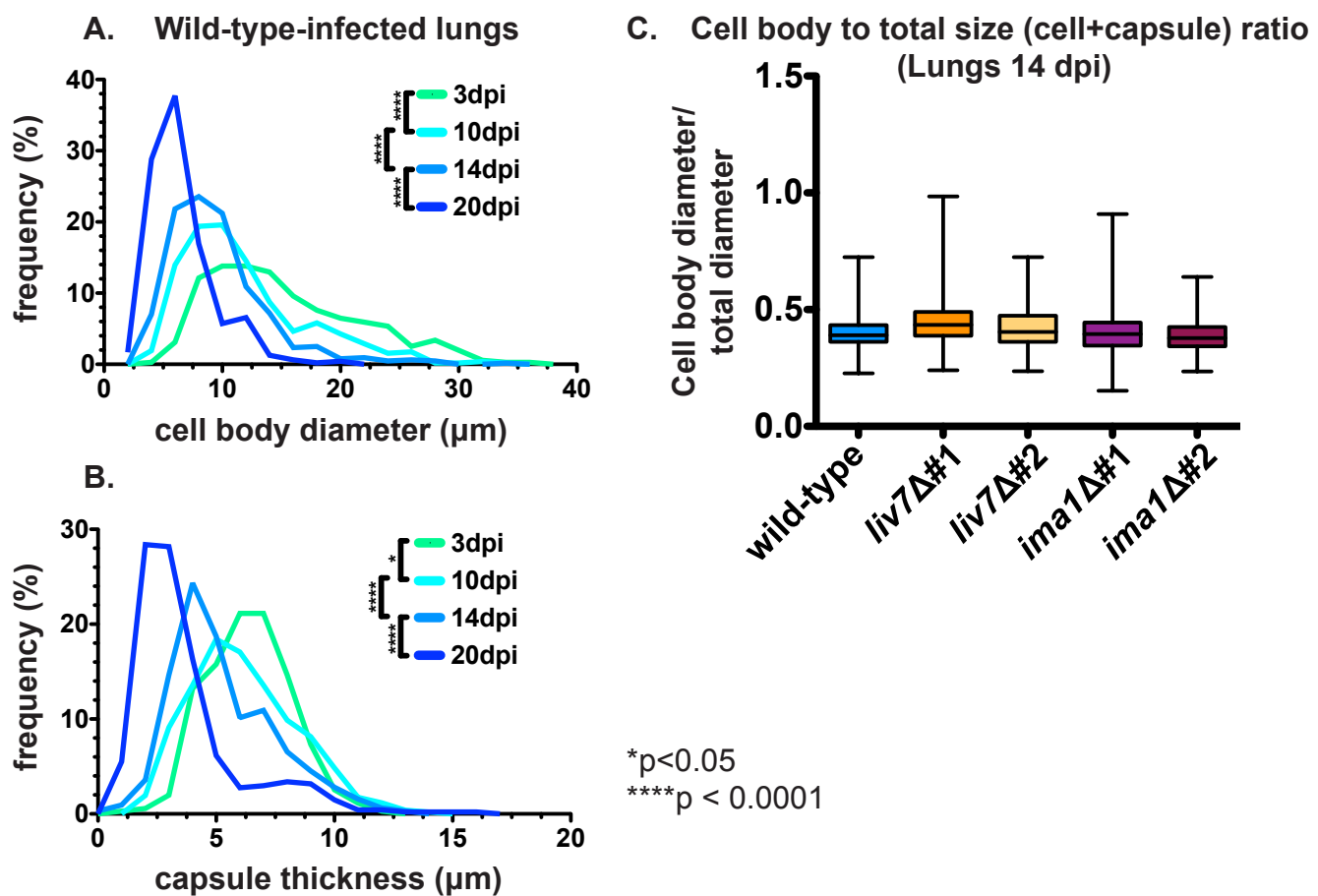


## Figure S7

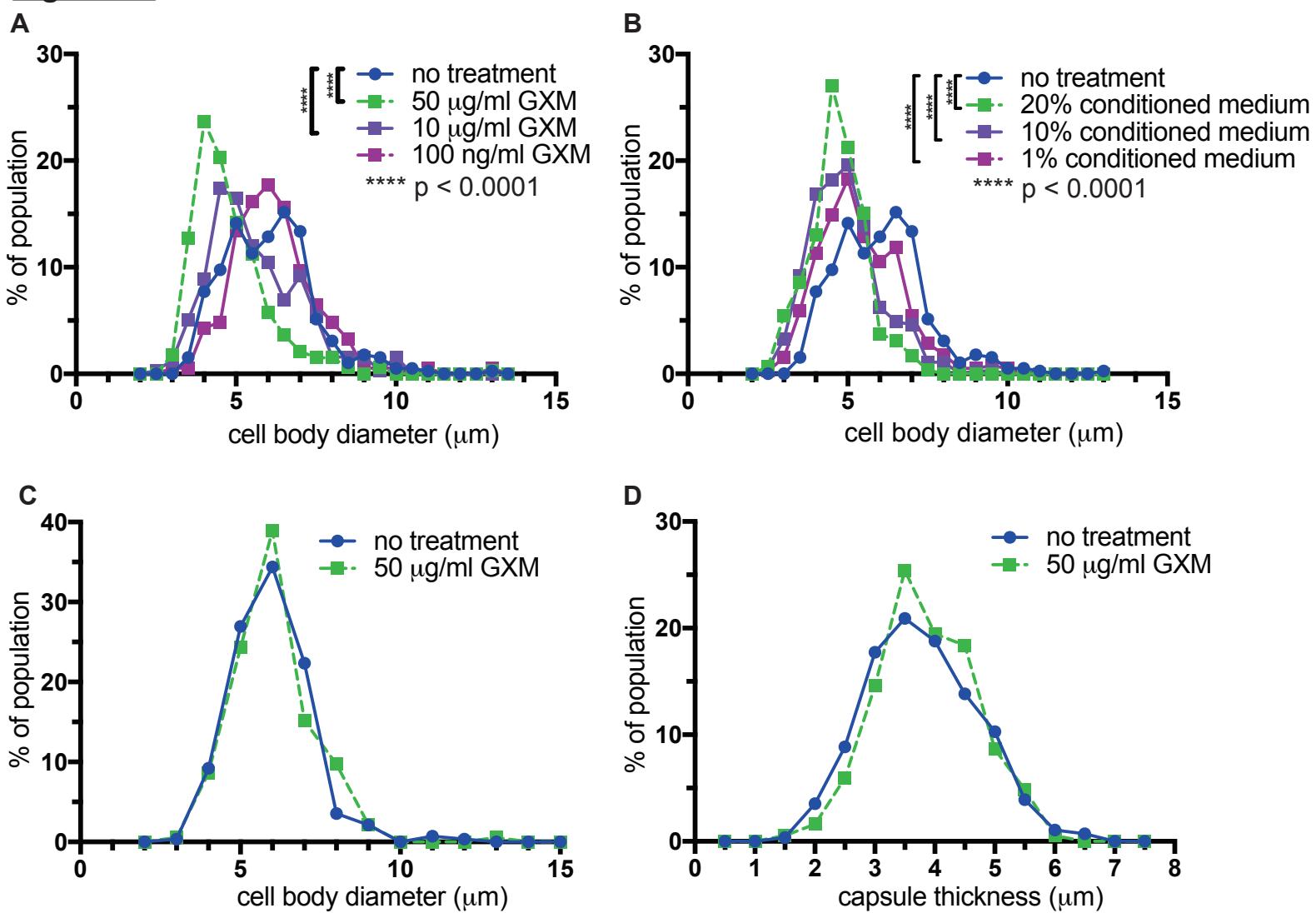
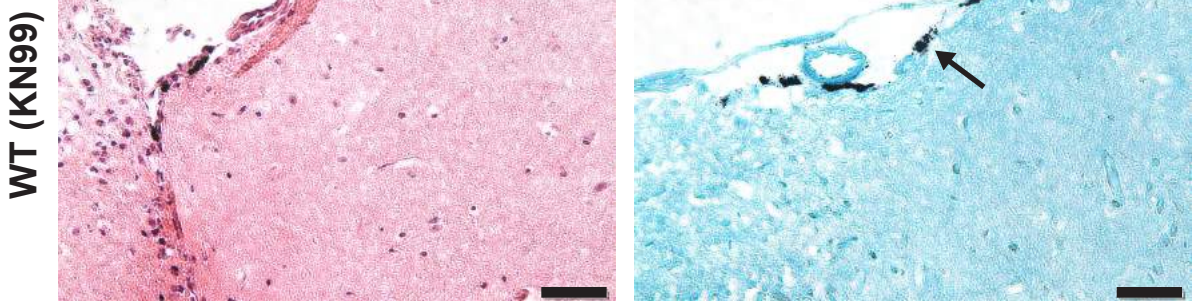
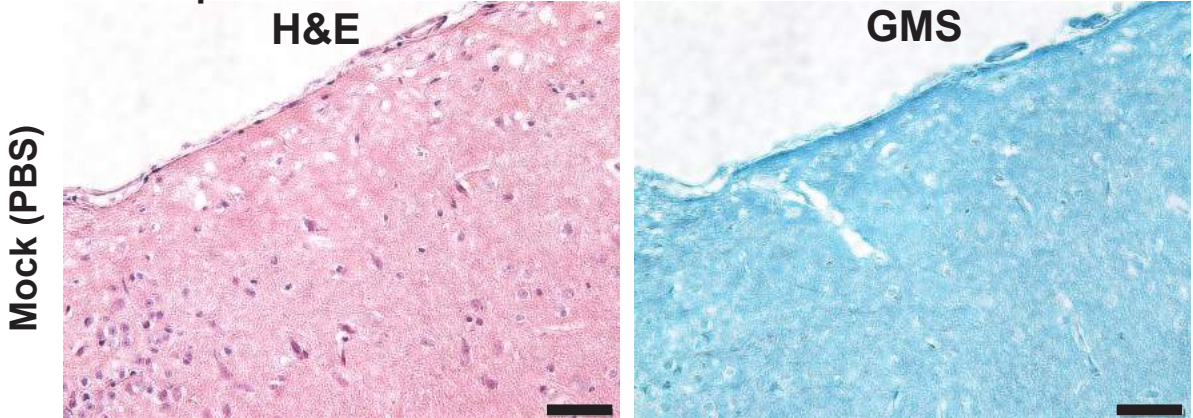
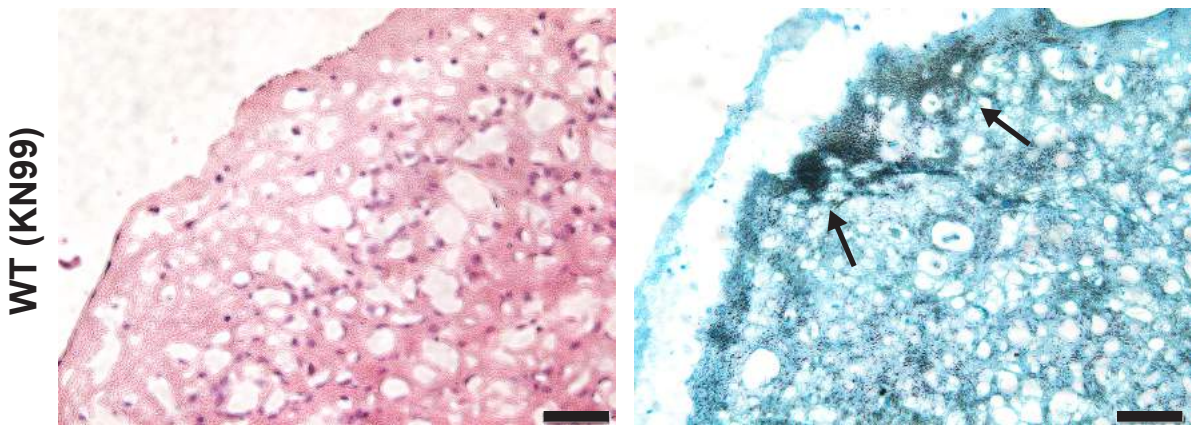
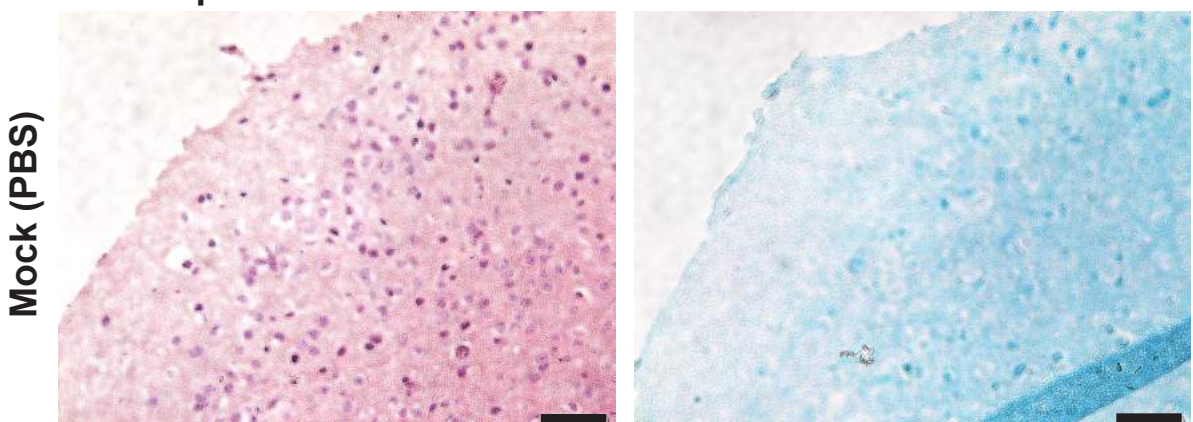


### Figure S8

A. 14 d.p.i.



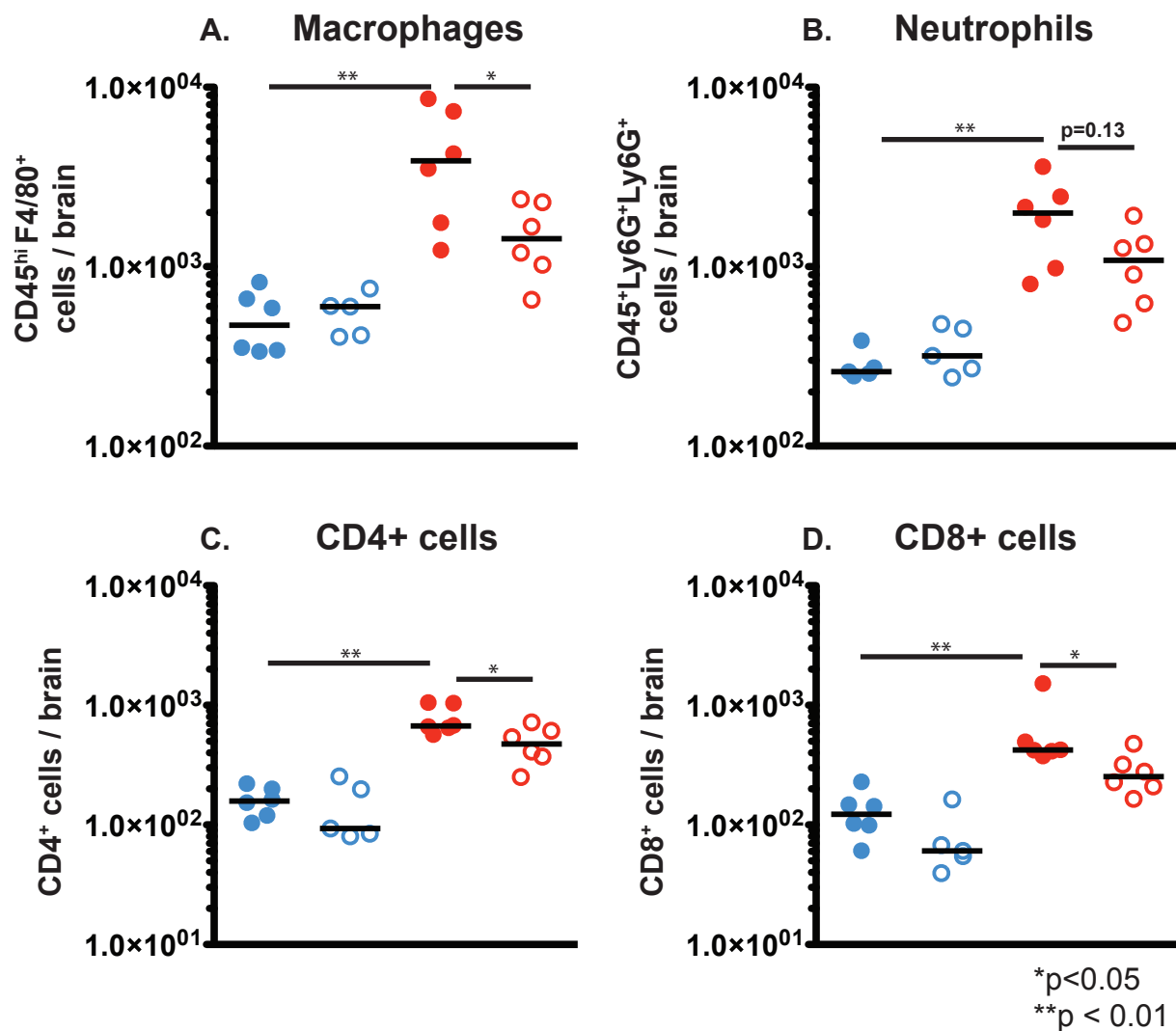
C. 21 d.p.i.



D.

scale=50  $\mu$ m

**Figure S9**



<b>(A) Gene deletion mutants with reduced exo-GXM in YNB</b>		
<b>CNAG</b>	<b>Molecular Function</b>	<b>Capsule</b>
CNAG_03171	WEE protein kinase	WT (++)
CNAG_04461	DNA helicase	++
CNAG_06673	conserved hypothetical protein	++
CNAG_04262	E3 ubiquitin-protein ligase (NRDP1)	++
CNAG_04443	conserved hypothetical protein	++

<b>(B) Gene deletion mutants with increased exo-GXM in 10 Sabouraud's, pH 7.3</b>					
<b>CNAG</b>	<b>Mutant Class</b>	<b>Molecular Function</b>	<b>Capsule</b>	<b>Urease</b>	<b>L-DOPA</b>
CNAG_00658	1	hypothetical protein	WT (++)	WT (++)	WT (++)
CNAG_03188	1	histone-lysine N-methyltransferase SETD2	++	++	-/+
CNAG_05838	1	Rho GTPase activating protein	+++	++	+++
CNAG_02189	1	alpha-amylase	++	++	++
CNAG_04756	1	hypothetical protein	++	++	++
CNAG_01551	2	transcription factor (Gat201)	-/+	++	++
CNAG_03582	2	pH response regulator protein (Rim20)	-/+	+++	-/+
CNAG_00375	2	histone acetyl transferase	-/+	++	-/+
CNAG_05690	2	histone deacetylase (Rpd3)	-/+	++	++
CNAG_04863	2	ESCRT-II complex subunit (Vps25)	-/+	+++	-/+
CNAG_03202	2	adenylate cyclase	-	++	-/+
CNAG_00761	2	coiled-coil domain-containing protein	+	+++	-/+
CNAG_06606	2	Rho family protein	+	+++	+
CNAG_05901	2	hypothetical protein	+	+	-/+
CNAG_02215	2	transcriptional activator (Hap3)	+	+	-/+